METHYLENE BLUE DEGRADATION IN WATER USING SOL-GEL MADE TiO_2 SUPPORTED OXIDE PHOTOCATALYSTS

A Thesis Submitted to
The Graduate School of Engineering and Sciences of
İzmir Institute of Technology
In Partial Fulfillment of the Requirements for the Degree of

MASTER OF SCIENCE

in Enviromental Engineering

by
Burcu KÖSEOĞLU

June 2011
İZMİR

We approve the thesis of Burcu KÖSEOĞLU

Date of Signature

…….. 6 July 2011
Assoc. Prof. Dr. Erol SEKER
Supervisor
Department of Chemical Engineering
İzmir Institute of Technology

…….. 6 July 2011
Assist. Prof. Dr. Yusuf SELAMET
Co-Supervisor
Department of Physics
İzmir Institute of Technology

…….. 6 July 2011
Assist. Prof. Dr. Ekrem ÖZDEMİR
Department of Chemical Engineering
İzmir Institute of Technology

…….. 6 July 2011
Prof. Dr. Levent ARTOK
Department of Chemistry
İzmir Institute of Technology

…….. 6 July 2011
Assoc. Prof. Dr. Oğuz BAYRAKTAR
Department of Chemical Engineering
İzmir Institute of Technology

....
Assoc. Prof. Dr. Sait Cemil SOFUOĞLU **Prof. Dr. Durmuş Ali DEMİR**

Head of the Department of Enviromental Engineering

Head of the Graduate School of Engineering and Sciences

ACKNOWLEDGEMENTS

I am particularly gratefull to my MSc supervisor Assoc. Prof. Dr. Erol Seker, for his friendliness, encouragement and support while supervising this research work and also for his original ideas. Also, special thanks go to my MSc cosupervisor Assist. Prof. Dr.Yusuf Selamet.

I would like to thank Mert Tunçer and Hüsnü Arda Yurtsever who have had supported me a lot throughout the study. Throughout my thesis study, they provided encouragement, sound advices and lots of good ideas.

I express my thanks to all laboratory co-workers; Selahattin Umdu, Emre Kılıç, Emel Dönmez, Selcan Ateş for their friendship and for taking my mind out of the work from time to time.

I am also very thankful to entire staff of the department of chemical engineering.

I wish to thank Serkan Kangal for helping me get through the difficult times, and for all the emotional support.

Finally my special thanks go to my mother Semiha Köseoğlu for her support.

ABSTRACT

METHYLENE BLUE DEGRADATION IN WATER USING SOL-GEL MADE TiO_2 SUPPORTED OXIDE PHOTOCATALYSTS

Pure TiO_2 and Fe^{3+} doped TiO_2 photocatalysts were synthesized by changing H_2O/Ti ratio, HCl/Ti ratios and calcination temperatures. Photocatalytic activities of the samples were determined for the degradation of methylene blue. The primary objective of this study is to narrow the band gap energies of the photocatalysts by changing preparation procedure and also doping with Fe^{3+} ions. Pure TiO_2 and Fe^{3+} doped TiO_2 photocatalysts were prepared by the sol-gel method, and also the impregnation method was applied for Fe^{3+} doping. The characterization of the samples was performed by using XRD and DRS techniques. Photocatalytic activities were measured by using UV-vis absorbance. This study shows that the heat treatment directly affected the crystallite size. Generally, crystallite size of the samples increased with calcination temperature and the heat treatment between 700 ºC and 800 ºC also resulted in crystalline phase transformation from anatase to rutile. TiO_2 samples prepared with H_2O/Ti ratio of 4 and HCl/Ti ratio of 0.15 calcined at 700 ºC and H_2O/Ti ratio of 4 and HCl/Ti ratio of 0.45 calcined at 800 ºC had only rutile phase.

Band gap energy is one of the important factors affecting the photocatalytic activities. In this thesis study, band gap energies of the TiO_2 samples were calculated using DR spectrums together with Kubelka Munk function. The DRS analyses showed that samples with rutile phase had the smallest band gap energies; in fact, the pure TiO_2 samples (H_2O/Ti ratio of 4 and HCl/Ti ratio of 0.45 calcined at 900 ºC) had the minimum band gap energy of 3.019 eV and the maximum photocatalytic conversion of 25% in 10 min and 93% conversion was reached in 15 h. In contrast, photocatalytic conversion decreased with doping with Fe^{3+} with excessive dissolution of iron ions.

ÖZET

SOL-JEL YAPIMI TiO_2 DESTEKLİ OKSİT FOTOKATALİZÖRLER KULLANILARAK SU İÇİNDE METİLEN MAVİSİ BOZUNUMU

Bu çalışmada H_2O/Ti oranı, HCl/Ti oranı ve kalsinasyon sıcaklıkları değiştirilerek, saf TiO_2 ve Fe^{+3} yüklenmiş TiO_2 nanopartikülleri sentezlenmiştir. Daha sonra tüm örneklerin fotokatalik aktiviteleri analiz edilmiştir. Bu çalışmanın ana amacı fotokatalizörlerin bant enerjilerini düşürmektir. Bunu sağlamak için örnekler sentezlenirken prosedürde bazı değişiklikler yapılmış ve Fe^{+3} iyonu yüklenmiştir. Saf TiO_2 ve Fe^{+3} yüklenmiş TiO_2 nanokatalizörleri sol-jel metodu ile hazırlanmış ve Fe^{+3} yüklemek için impregnasyon metodu uygulanmıştır. Hazırlanan örneklerin karakterize edilmesi XRD ve DRS teknikleri ile yapılmıştır. Metilen mavisi bozularak, örneklerin fotokatalitik aktiviteleri incelenmiş ve UV-vis soğurma ile analiz edilmiştir. Bu çalışma ısıl işlemin kristal boyut üzerinde doğrudan etkili olduğunu göstermiştir. Genel olarak, kalsinasyon sıcaklığı artarken örneklerin kristal boyutları da artmıştır. Ayrıca, ısıl işlem faz oluşumunu da etkilemektedir. 700-800 ºC arasında anatazdan rutile faz dönüşümü olmaktadır. H_2O/Ti oranı 4'e eşit ve HCl/Ti oranı 0.45'e eşit olan ve 800 ºC kalsine edilmiş TiO_2 örneklerinde rutil faz gözlemlenmiştir. Ayrıca, bant enerji değerleri örneklerin fotokatalitik aktiviteleri için önemlidir. Çünkü, küçük bant enerjisine sahip TiO_2 fotokatalizörleri görünür ışık aralığında çalışabildikleri için fotokatalitik reaksiyonlarda daha aktiftirler. Bu tez çalışmasında TiO_2 örneklerinin bant enerjileri DR spektrumları, Kubelka Munk fonksiyonu ve Polymath programı kullanılarak hesaplanmıştır. Sonuçlara göre, rutil fazlı örnekler daha küçük bant enerjilerine sahiptir. Ayrıca, en düşük bant enerjileri saf TiO_2 örneklerinden elde edilmiştir. TiO_2-w:4-a:0.45-T:900 örneği minimum bant enerjisine sahiptir, değeri 3,019'dur ve maksimum fotokatalitik verimi, %25, göstermiştir. Ayrıca, Fe^{+3} yükü arttıkça fotokatalitik verim düşmektedir. Bu sonuç, TiO_2 yüzeyindeki Fe^{+3} safsızlığının örneklerin fotokatalitik verimini düşürdüğünü göstermektedir. Maksimum fotokatalitik aktivite gösteren TiO_2-w:4-a:0.45-T:900 örneğinin zamana bağlı fotokatalitic verimi çalışılmıştır. 15 saat içinde %93 bozulma göstermiştir.

TABLE OF CONTENTS

LIST OF FIGURES

LIST OF TABLES

CHAPTER 1

INTRODUCTION

During the past several decades, fast and relatively uncontrolled population growth and also industrial, agricultural and technological developments have adversely affected the environment and human health. Especially wastewater effluents of industrial manufacturing companies contain toxic organic compounds. Additionally, the combustion of fossil fuels has caused global warming due to the increase of CO_2 concentration in the atmosphere

The world is facing difficult environmental problems and also diminishing fossil fuels. Moreover, attempts to compensate the effect of decreasing of traditional fossil fuel resources have resulted in new emerging technologies, such as fuel cell technologies, but these new technologies seem to create their own pollution problems. For instance, methanol fuel cells could cause methanol spill contamination. Methanol occurs naturally in humans, animals and plants. But, overdose becomes harmful for animals and humans. Oral LD50 values for methanol in animals are 0.4 g/kg for mice, 6.2 to 13 g/kg for rats, 14.4 g/kg for rabbits, and 2 to 7 g/kg for monkey. The LD50 for dermal application to rabbits is 20 mL/kg (approximately 16 g/kg) (EPA 1994).

Methanol is highly mobile in soil (EPA 1994). This indicates that it easily reaches water sources. Due to its high miscibility in water, the contamination damages natural life in the water streams, such as fish and plant populations. For example, northern squawfish dies upon 24 h of exposure to 0.01 g/L of methanol, carp dies upon 24 h of exposure to 7.9 g/L , goldfish dies upon 48 of exposure to 2.1 g/L.

Moreover, with the rapid development of the printing and dye industry, the effluents of these industries have become one of the most important water pollution sources. The printing and dye industries' effluents are very complex, usually containing some remaining dyes, some sizing agents, some surfactants and some accessory ingredients amongst the others. Besides, many dyes are very toxic and cause serious damage to human beings even at very low concentrations. Traditional wastewater treatments for printing and dyeing plants' effluents are mainly physical, chemical and

biochemical methods. Moreover, with the rapid development of the textile industry in recent years, more and more new types of dye have been produced, such as methylene blue (Jian-xiao et al. 2011). TiO_2 is able to photocatalyze the complete oxidative mineralization of methylene blue by O_2. It is also able to photooxidize acid blue dye used in textile industry according to mechanism of;

$$C_{16}H_{18}N_3SCl + 25.5O_2 \xrightarrow{TiO_2;\ air} 16CO_2 + 6H_2O + 3HNO_3 + H_2SO_4$$

(Source: Salem et al. 2000)

Furthermore, it is used as a stain in bacteriology and also an oxidation-reduction indicator, i.e. an antidote to cyanide, and in veterinary, it is used as antiseptic. Methylene blue is a heterocyclic aromatic chemical compound with the molecular formula $C_{16}H_{18}N_3SCl$ (Jian-xiao et al. 2011). Molecular structure of methylene blue is shown in the Figure 1.1.

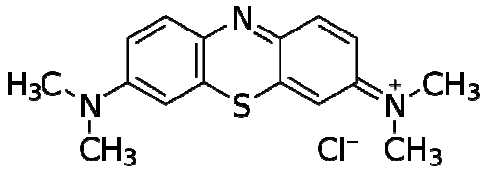

Figure 1.1. Crystal structure of methylene blue
(Source: Jian-xiao et al. 2011)

Today, chemical contamination of water streams has become crucial issue. To prevent this problem wastewater treatment plays an important role. For this reason, heterogeneous photocatalysis can be applied to remove contaminants existing in the wastewater effluent (Sobczynski and Dobosz 2001).

Catalysis under light irradiation is called photocatalysis. Heterogeneous photocatalysis includes kind of reactions such as organic synthesis, water splitting, photoreduction, hydrogen transfer and metal deposition, disinfection and anti cancer therapy, water treatment, removal of gaseous pollutants, etc. (Colmenares et al. 2009). It has become an increasingly viable technology in environmental decontamination. Photocatalytic oxidation of organic compounds in the environment is derived by semiconductor materials such as TiO_2, ZnO, GaP, SiC CdS, and Fe_2O_3 (Sayılkan et al. 2006). Among the various semiconductor materials, TiO_2 is the most widely used

photocatalyst when compared to other photocatalysts due to its low cost, non-toxicity, high activity, large chemical stability, very low aqueous solubility and environmentally friendly characteristics (Tseng 2010; Thiruvenkatachari et al. 2007).

In 1972, the photocatalytic activity of TiO_2 was discovered by Fujishima and Honda (Leary et al. 2010; Song et al. 2007). Titania-asisted photocatalytic oxidation is an alternative method for purification of air and water streams. Also, in this way of water splitting, the driving force for electrons is provided by energy of the light. When TiO_2 is exposed to light, photocatalytic reaction is initiated. In fact, an electron which is in the filled valence band becomes excited and jumps to the empty conduction band upon the exposure to the light. Hence, the photon energy, $h\upsilon$, which equals or exceeds the band gap of the semiconductor photocatalyst leaves a hole in the valence band; i.e. electrons (e^-) and positive holes (h^+) are produced as shown in Figure 1.2 (Colmenares et al. 2009). The following chain reactions have been accepted to occur during the heterogeneous photocatalysis:

(1) Photoexcitation: $TiO_2 + h\upsilon \rightarrow e^- + h^+$

(2) Oxygen ionosorption: $(O_2)\ ads + e^- \rightarrow O_2^{\bullet -}$

(3) Ionization of water: $H_2O \rightarrow OH^- + H^+$

(4) Protonation of superoxides: $O_2^{\bullet -} + H^+ \rightarrow HOO^{\bullet}$

The hydroperoxyl radical formed in (4) has also scavenging properties similar to O_2 thus it making the lifetime of photohole two times longer:

(5) $HOO^{\bullet} + e^- \rightarrow HO_2^-$

(6) $HOO- + H+ \rightarrow H_2O_2$

Both of the oxidation and reduction reactions occur at the surface of the photoexcited semiconductor photocatalyst (Colmenares et al. 2009).

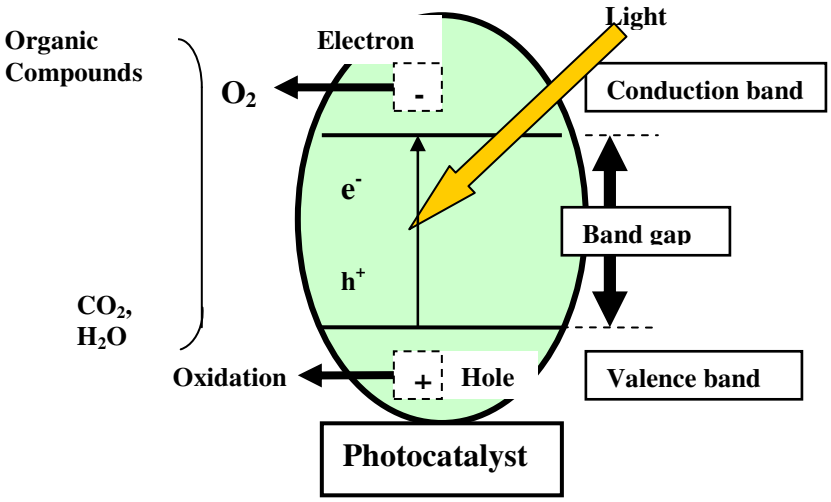

Figure 1.2. Operation of a photochemical excited TiO_2 particle

Energy difference between the valance and conduction band is called band gap energy. The lower edge of the conduction band and upper edge of the valence band are presented along with the band gap in electron volts (Ahmmad 2008). The energy band diagrams of some semiconductors are shown in Figure 1.3.

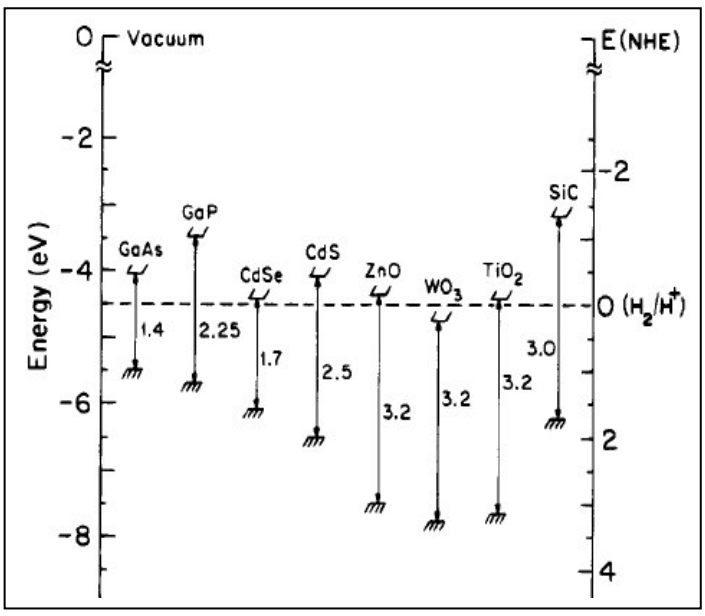

Figure 1.3. Energy diagram of typical semiconductors
(Source: Ahmmad 2008)

The band gap of a semiconductor is always one of two types: direct band gap or indirect band gap. Direct band gap semiconductors can absorb light energy efficiently. Since, the photon absorption process requires no assistance from lattice vibrations. Upon photon absorption, the electron is excited directly from the valence into the conduction band without changing their momentum. Compounds of elements from groups III and V in the periodic table are known direct band gap semiconductors, such as gallium arsenide and indium phosphide. In indirect bandgap semiconductors such as Si or Ge, the photon absorption requires the absorption or emission of a phonon (Kersauson et al. 2010).

Both direct and indirect bandgaps are affected by the nature and concentration of the incorporated impurities, but no systematic study of this property has appeared in the literature (Qui et al. 2007).

TiO_2 is commercially available and easy to prepare in the laboratory. Their catalytic activity can be improved by increasing its specific surface area and the crystallite size. The smaller catalysts have the large specific surface area (Su et al. 2004). They have white color. Thus, they have no absorption in the full spectra of the visible range (Fujishima et al. 2005).

TiO_2 exist in three major crystalline forms; anatase, rutile and brookite. Only rutile and anatase are commonly used in photocatalysis since brookite phase is not stable above 150 ^oC. Crystalline structures of TiO_2 are shown in the Figure 1.4.

The anatase form has the free electrons in its crystal lattice, thus it is an n-type semiconductor. In fact, anatase has been reported to give the best combination of photoactivity and photostability (Park et al. 2005; Colmenares et al. 2009).

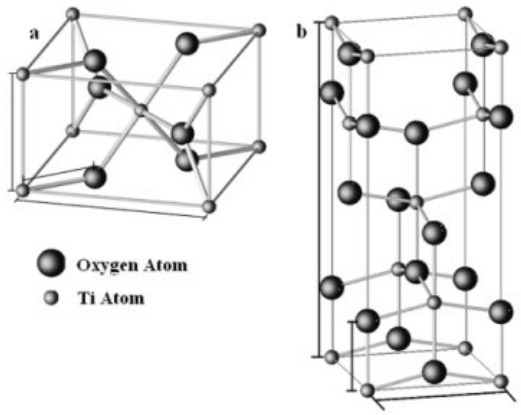

Figure 1.4. Crystallographic unit cell structure of TiO2 with a) rutile and b) anatase Structures (Source: Banerjee 2011).

Band gap energies of some semiconductors are given in the Table1.1. The band gap value is 3.0 eV for rutile and 3.2 eV for anatase phase; they both absorb only in ultraviolet region. However, the rutile type can absorb the light that is slightly closer to visible light region.

Table 1.1. Band gap energies of some semiconductors

Semiconductor	Eg (eV)
Si	1.1
Fe_2O_3	2.3
CdS	2.5
WO_3	2.8
TiO_2 (rutile)	3.0
TiO_2 (anatase)	3.2
ZnO	3.2
SnO_2	3.5

3.2 eV which is band gap energy of anatase, corresponds to a wavelength of 388 nm. Practically, TiO_2 photoactivation takes place in the range of 300–388 nm (Colmenares et al. 2009). So that, only UV light can be used for titania. Therefore, this band gap energy makes it impossible to use the full spectra of the visible light. In order words, it requires UV light to activate TiO_2 and about 3-5% energy of the solar spectrum which was the range of 400-800 nm is used. Thus, this absorption edge needs to be extended to the visible range in order to effectively use the direct sunlight. Thus, band gap needs to be narrowed by doping transition metal ions, such as Fe, Ag, V, Cr and Ni, and noble metals, such as Pt, Au, Pd, Os and Hg, and rare earths metals, such as La^{3+}, Nd^{3+}, Sm^{3+}, Eu^{3+}, Gd^{3+}, and Yb^{3+}; also some metal oxides, such as MgO, Fe_2O_3, CuO and ZnO (Wang 2010; El-Bahy et al. 2008; Paola et al. 2004). Among these elements, Fe is very cost-effective and can contribute to shifting the absorption edge of TiO_2 into visible light range (Wang 2010).

In this study, the focus is on synthesizing TiO_2 and Fe doped TiO_2 for use in photocatalytic degradation of methyelene blue with the intention of reducing the band gap energy of the TiO_2 photocatalysts so that, the wavelength range in which photocatalytic activity is observed shifts to the visible light spectra.

This thesis contains five chapters. In chapter one, a general introduction to environmental pollution sources, their effects and the significance of water treatment and the general introduction to photocatalysts and also the aim of this thesis are introduced. In chapter two, a literature survey on the types of TiO_2 materials and their photocatalytic properties, and also the material preparation methods are presented. In chapter three, the specifications and pretreatment procedures of the chemicals used in this thesis and also the material preparation methods, such as the single step sol-gel method, is explained in details. Also in this chapter, the material characterization methods, such as X-Ray diffraction and the diffuse reflectance spectroscopy are given. In chapter four, effects of acid and water amounts used in sol-gel method and calcination temperature on the material properties, such as crystallite sizes, crystalline phases and band gap energies, are presented and it is discussed if there is a relationship between the photocatalytic degradation and the material properties of the TiO_2 and Fe^{3+} doped TiO_2 materials studied in this thesis. Finally, the conclusions and some recommendations are listed in chapter five.

CHAPTER 2

LITERATURE SURVEY

2.1. Photocatalysis

Photocatalysis is a catalytic reaction which requires light energy. Photosynthesis which occurs in plants is commonly known example of photocatalytic reaction. During this process, plants produce oxygen by oxidizing water and reduce CO_2 by solar energy. Inspired by this process, Fujishima et al. investigated photoelectrolysis of water using light energy (Fujishima et al. 2000). CdS, Cu_2O, Fe_2O_3, WO_3 can absorb visible light. But this attempt failed, since no semiconductors have the required band gap energy, chemical stability, and photocatalytic activity together (Fujishima et al. 2005). TiO_2 had greater photocatalytic efficiency than α-Fe_2O_3, ZrO_2, CdS, WO_3 and SnO_2 (Thiruvenkatachari et al. 2007). Anandan et al. prepared ZnO semiconductor by doping lanthanum for the degradation of 2,4,6-TCP in aqueous suspension. They found that the relative photonic efficiency and photocatalytic activity of doped ZnO is more than the pure ZnO and pure TiO_2 (Anandan et al. 2007). However, ZnO had a higher activity (although the surface area is less) than TiO_2, the later was photochemically more stable in aqueous media (Thiruvenkatachari et al. 2007). It is also noted that, TiO_2 is an excellent material for photocatalytically breaking down organic compounds. As an example to this, if catalytically active TiO_2 powder put into a shallow polluted water, and exposed to sunlight, water is purified (Fujishima et al. 2000).

2.2. Sol-gel Synthesis Method of Photocatalysts

There are several kinds of TiO_2 powders preparation methods; for instance chemical precipitation, microemulsion, hydrothermal crystallization and sol-gel (Su et al. 2004). Due to its low-cost, low-temperature processing, and good shaping ability, sol-gel is the most commonly used technique (Wang et al. 2010). Many researchers prefer the sol-gel method in the synthesis of TiO_2 (Hsiung 2007; Thiruvenkatachari 2007; Al-Salim et al. 2000; El-Bahy 2008).

Moreover, photocatalytic activity of TiO_2 strongly depends on the crystalline structures which are anatase, rutile and brookite. For example, anatase phase of TiO_2 are generally found to be more active than rutile phase (Sun et al. 2003). Crystalline structure can be controlled by heat treatment after sol-gel preparation. Very high calcination temperatures cause aggregation and phase transformation (Su et al. 2004). Thus, calcination temperature affects the microstructures of TiO_2 photocatalysts. Su et al. investigated microstructural and chemical properties of TiO_2 by using sol-gel methods with changing calcination temperatures. They calcined to prepare TiO_2 photocatalysts at 400 to 700 °C. C. Su et al. reported that the obtained crystalline phases were all anatase for calcination temperature of 400 °C. Moreover, they observed, when calcination temperature increased, the phase transformation occurred from anatase to rutile. When TiO_2 was calcined at 500 °C and above, TiO_2 became a mixture of anatase and rutile.

2.3. TiO_2 Photocatalysts

Beginning with 1960s, TiO_2 was found to be a viable photocatalyst (Fujishima 2000). TiO_2 can exist as an amorphous layer and also in three crystalline phases: anatase (tetragonal), rutile (tetragonal) and brookite (orthorombic) (Hasan et al. 2008). The position of oxygen ions on the exposed crystalline surface of anatase shows a triangular arrangement, allowing effective absorption of organics (Thiruvenkatachari 2007). Whereas, the positions of titanium ions create a favorable reaction condition with the absorbed organics. However, this favorable structural arrangement is not available for rutile structure. This is one of the reasons why anatase has higher photocatalytic activity than rutile. However, Thiruvenkatachari suggested that a pure anatase sample would not necessarily lead to the best photocatalytic performance. The presence of rutile phase introduces mesoporosity and a wider pore size distribution. These factors may be responsible for the increased catalytic activity. So for that reasons, a mixture of anatase and rutile would be the best combination to achieve maximum photocatalytic efficiency (Thiruvenkatachari 2007).

For example, commercial TiO_2 of Degussa P-25 TiO_2 (mixture of 70% anatase, 30% rutile material) gives better degradation efficiency compared to other forms (Yamazaki et al. 2000). The effect of particle size on the photocatalytic activity can be

interpreted in terms of surface area (anatase=10 m^2/g, rutile=20 m^2/g, Degussa P25=50 m^2/g) (Xu et al., 1999). Generally, smaller particle size provides larger surface area; hence, the higher activity. This can be explained in terms of an increase in the number of active sites per square meter, as well as greater adsorbability of the pollutants on the catalyst surface (Thiruvenkatachari 2007).

The enhanced photocatalytic activity of nanosize TiO_2 has been attributed to the quantum confinement (quantum size) effect and the enlargement of surface-to-volume ratios (Hsiung et al. 2007; Chan et al. 1998). Hsiung et al. studied about the chemical structure of nanosize TiO_2, synthesized by the sol–gel method and compared it with commercial TiO_2 catalysts, and analyzed photocatalytic activity by degradation of methylene blue (MB). They calcined synthesized TiO_2 nanoparticles at 473 and 673 K for 1 h. They reported that there was only anatase phase and avarage particle size of TiO_2 photocatalyst was 8.8 nm.

Al-Salim et al. reported that the impact of incorporating alkaline earth ions, which were Ca, Sr and Ba ions, (up to 20 mol %) on the physicochemical properties of sol-gel-prepared titania powders. They kept calcination temperature at maximum 600 ºC to avoid rutile formation. They found that at this temperature undoped sample crystallized as anatase without rutile formation. It is known that dopants can delay the anatase to rutile transformation, allowing >95% anatase to be obtained, even after high temperature calcination. Band gaps were determined by the Kubelka-Munk functions in their study. It is reported that when Ca^{+2} ion concentrations in the samples increased, crystallite size reduced, band gap values increased (Al-Salim et al. 2000). A larger band gap results in an increased rate constant for the charge transfer, which can result in improved photoefficiencies. Reaction rate enhancement can also be due to the increased migration of electrons and holes to the semiconductor surfaces in smaller particles (Hoffman et al. 1995).

El-Bahy et al. dealt with the enhancement of TiO_2. In their study, they doped rare earth elements for maximizing the efficiency of photocatalytic reactions. Lanthanide ions which were La^{3+}, Nd^{3+}, Sm^{3+}, Eu^{3+}, Gd^{3+}, and Yb^{3+} were used for doping elements. All samples were synthesized by a sol-gel method. They reported that all of the doped TiO_2 nanoparticles have anatase phase and no diffraction peaks of lanthanide oxides in the XRD patterns. It was claimed that lanthanide oxides were well dispersed within TiO_2. Also, they reported that all the studied lanthanide ions inhibit the phase transformation from anatase to rutile during calcinations even at high

temperatures which was 550 ºC. They calculated the crystallite size of pure TiO_2 and doped TiO_2 ranging from 20.3 to 29.5 nm; the lanthanide/TiO_2 had lower crystallite size than pure TiO_2. This reduction in crystallite size was proposed due to segregation of the dopant cations at the grain boundary which inhibits the grain growth by restricting direct contact of grains (El-Bahy et al. 2008).

Lanthanide ions-doped titania nanoparticles have the lower bandgap energy than pure TiO_2 nanoparticle. This was definitely effect of the semiconduction properties of the prepared nanoparticles. El-Bahy et al. analyzed and reported surface area of the lanthanide/TiO_2 and pure TiO_2 samples. According to their results, surface area and mesopore volume of the lanthanide ions-doped TiO_2 were greater than the pure TiO_2. They claimed that TiO_2 structure is not affected by doping with lanthanide ions as revealed in XRD spectrum, the increase of surface area and mesopore volume was observed for the lanthanide ions-doped TiO_2 (El-Bahy et al. 2008).

Paola et al. studied the physicochemical characterization and photocatalytic activity of TiO_2 powders loaded with some transition metal ions with different amounts. These were Cr, Co, Cu, Fe, Mo, W and V. They used wet impregnation method to prepare the titania powders (Paola et al. 2004). Surface active sites and surface area are important since, chemical reaction occurs at the surface (Leary 2010). Paola et al. analyzed and reported the specific surface areas of samples. They claimed that surface areas of the samples decreased with increasing the amount of loaded metal (Paola et al. 2004).

Wang et al. prepared Fe^{3+} doped TiO_2 films deposited on fly ash cenosphere (FAC), by sol-gel method. The molar ratios of Fe to Ti were 0.005%, 0.01%, 0.05%, 0.1%, and 0.5%. No characteristic peak of iron oxides or Fe_xTiO_y phases were observed even in the 1% Fe/Ti molar ratio sample in reported XRD pattern, indicating the high dispersion of Fe^{3+} in TiO_2 crystal lattice without significant changing of the titania nature. According to Wang et al, calcined temperature had a great influence on crystalline forms of their synthesized photocatalysts. With increasing calcination temperature from 350 ºC to 450 ºC, amorphous TiO_2 turned into anatase phase and intensity of peaks in response to anatase phase increased greatly at (101) crystalline plane. However, rutile phase was detected when temperature was raised to 650 ºC. In comparison to different Fe–TiO_2/FAC photocatalysts, the sample of 0.01% Fe/Ti molar ratio showed the best photocatalytic ability (Wang et al. 2010).

Vijayan et al. studied with the photocatalytic activity of pure and Fe doped nanocrystalline TiO_2. They doped Fe in different weight percentages which were 0.3, 0.5, 0.7 an 1 wt.%. TiO_2 was prepared using sol–gel followed by hydrothermal methods, calcined at 500 ºC and tested for the photocatalytic oxidative degradation of 2,4,6-trichlorophenol in their study. They examined the phase composition and the crystallite size of the prepared samples by using X-ray diffraction method. They reported that all of the synthesized samples were anatase phase and also metals were well dispersed due to absence of diffraction peaks corresponding to metals. Average crystallite size of TiO_2 was estimated using the Scherrer's equation by the Vijayan et al. Scherer Formula is given by Equation (3.1) in Chapter 3. According to the results, they asserted that the metal doping restricted crystallite growth and reduced the size (Vijayan et al. 2008).

Song et al. dealt with the preparation and characterization of the pure and Fe doped TiO_2 gelatins. They doped Fe in the TiO_2 in order to reduce the band gap of the photocatalysts. They prepared gelatins by the sol-gel method. Obtained gel firstly dried at 80 °C and after that calcined at different temperatures which were 300 °C, 400 °C, 500 °C and 600 °C in their study. They analyzed the phase structure and the crystallite size of the samples. The X-ray diffraction (XRD) patterns of pure TiO_2 was reported in their study for 300 °C, 500 °C and 600 °C calcination temperature. According to their XRD results, they claimed that Fe-doped TiO_2 samples were amorphous after drying at 80 °C. At 300 °C the sample only contained anatase phase. At 500 °C, a small amount of rutile phase was observed. When the temperature was increased to 600 °C, it was realized that most of the sample transformed into rutile phase. Moreover they calculated the grain size of the samples with the Scherer Formula. They found the grain sizes as 8.25 nm and 19 nm for 300 °C and 600 °C, respectively. Furthermore, they declared that, there was no characteristic peaks of impurities were observed in the XRD pattern, which indicated that the products were high purity and the Fe^{3+} dissolved in the lattice of crystallized TiO_2 completely. Additionally, they measured specific surface area of the Fe-doped $TiO_2$and interpreted the effect of temperature on specific surface area of Fe-TiO_2. They professed that with increasing temperature, specific surface area of Fe-TiO_2 increased (Song et al. 2007).

Qui et al. dealt with preparation and characterization of the Ce^{4+} and Fe^{3+} doped TiO_2 (anatase and rutile) nanoparticle photocatalysts obtained by a sol-gel method. Then, they carried out its utilization for the photocatalytic degradation of nitrite in water. The calcination temperature was very important on the phase compositions of

TiO_2 nano powders. They used 400, 450, 550 and 700 °C temperatures in the preparation. Only the peaks of anatase phase of TiO_2 were observed when 400 °C was used and that of rutile phase was not detected. While the peak of rutile crystal plane indices (101) was observed in the XRD patterns of the sample calcined at 450 °C. It was showed that the beginning of formation of rutile and the phase transition from anatase to rutile started at this temperature. The formation of the mixture of anatase and rutile phase of TiO_2 calcined at 450 °C and 550 °C was observed clearly. The peak intensity of anatase was decreased with the raising of the calcination temperature. Anatase was transformed directly to rutile phase of TiO_2 calcined at 700 °C. The phase transition from anatase to rutile and crystallization of particles were improved by increasing calcination temperature.

Since, the use of conventional powder catalysts results in disadvantages of stirring during the reaction and of separation after the reaction, some researchers coated the catalysts as thin films by the dip-coating method (Yu 2000; Hasan et al. 2008).

There are many deposition methods used to prepare TiO_2 thin films, such as electron-beam evaporation, ion-beam assisted deposition, DC reactive magnetron sputtering, RF reactive magnetron sputtering, sol-gel method, chemical vapor deposition and plasma enhanced chemical vapor deposition (Hasan et al. 2008).

Hasan et al. prepared TiO_2 films by RF reactive magnetron sputtering, in their work. They checked the XRD patterns of TiO_2 films which were as-deposited at room temperature and annealed at different temperatures. From their results, they reported that all the films were polycrystalline having anatase phase only. From diffraction patterns, they reported that the films as-deposited, annealed at 300 °C, 400 °C, 500 °C exhibited characteristic peaks of anatase phase with crystal planes of (101), (200) and (211). For the sample annealed at 600 °C, other characteristic peaks of anatase with crystal planes of (204) and (220) appeared, but the intensity of these peaks was very weak. According to all these results, peak intensities of anatase planes increased slightly with increasing annealing temperature (Hasan et al. 2008). Hasan et al. estimated the direct and indirect band gap energies in their study. They reported that the indirect optical band gap increased from 3.39 eV to 3.42 eV with the increase of annealing temperature up to 600 °C. Also, estimated direct band gaps were reported in their study. The direct optical band gaps for the as-deposited films and annealed at 300 °C, 400 °C, 500 °C and 600 °C was reported 3.67, 3.68, 3.70, 3.72 and 3.68 eV respectively (Hasan et al. 2008).

2.3.1. Optical Properties of TiO_2

Hasan et al. analyzed the optical properties of TiO_2 films. They checked the transmittance of deposited and annealed TiO_2 films. They observed and reported that about 85% in the visible region with respect to reference blank glass substrate. Also, they claimed that annealing caused a slight decrease in transmittance with the increased of annealing temperature. The films annealed at 600 °C showed a significant decrease in visible light transmittance. They reported that average transmittance of as-deposited TiO_2 films in the visible spectral region was above 80% for films on glass and quartz substrate. TiO_2 films annealed at a higher temperature showed a lower transmittance. Because annealing treatment causes a film surface to be more rough which scatters light (Hasan et al. 2008).

Vijayan et al. studied diffuse reflectance spectrums of Fe doped and undoped TiO_2. They reported that the Fe–TiO_2 showed photo absorption at 410–445 nm. When compared with the undoped TiO_2, doping ions caused significant absorption shifts into visible region. Furthermore, calculated band gap energies change from 3.10 to 2.72 eV as loading level was increased (Vijayan et al. 2008).

2.3.2. Photocatalytic Activity of TiO_2

Recent photocatalysis researchers are dominated by the use of TiO_2 photocatalysts. They evaluated the photoactivity of modified photocatalysts by the degradation of different organic compounds. These studies are listed in the Table 2.1.

Table 2.1. Types of TiO_2 used in the degradation of organic contaminant

Research done by	Organic contaminant	Type of TiO_2 photocatalyst
Al-Salim et al. (2000)	Oxalic Acid	Alkaline Earth Ions/TiO_2
Paola et al. (2004)	Methanoic Acid/Ethanoic Acid/Benzoic Acid	Transition Metals/TiO_2
El-Bahy et al. (2008)	Direct Blue Organic Dye	Lanthanide/TiO_2
Qui et al. (2007)	NO_2	TiO_2 - Fe/TiO_2
Song et al. (2007)	Methyl Orange	TiO_2 - Fe/TiO_2
Hsiung et al. (2007)	Methylene Blue	TiO_2 - Fe/TiO_2
Vijayan et al. (2008)	2,4,6-trichlorophenol	TiO_2 - Fe/TiO_2
Wang et al. (2010)	Methylene Blue	Fe/TiO_2

Hisung et al. examined the photocatalytic activity of the TiO_2 photocatalyst by the degradation of methylene blue. In their study, at the absence of TiO_2, about 20% of MB was degraded under UV–vis radiation for 90 min. Then, they studied with commercial TiO_2, approximately 42% of MB degraded. They claimed that their synthesized TiO_2 photocatalyst, degraded about the 90% of MB in the first 20 min (Hsiung et al. 2007). This is radically high activity for synthesized TiO_2 photocatalyst.

Vijayan et al. performed the photocatalytic activity of Fe doped and undoped TiO_2 by 2,4,6-trichlorophenol, in a slurry batch reactor. They analyzed the influence of metal doping amounts on the activity. They observed that the photodegradation efficiency of Fe–TiO_2 increased with increasing Fe concentration, reaching a maximum at 0.5 wt.% Fe. The optimal amount of Fe on TiO_2 was found to be 0.5 wt.% in their study. However, it was also reported that when the photocatalytic activity of undoped TiO_2 and 1 wt.% Fe–TiO_2 were compared, undoped TiO_2 showed better catalytic activity than 1 wt.% Fe. It was reported that at low doping level of metal, photogenerated holes and electrons were well separated, thereby increasing the efficiency of the catalyst (Vijayan et al. 2008).

Paola et al. also analyzed photoreactivity of the samples. In order to do this, they checked the photodegradation of three different organic acids which were methanoic acid, ethanoic acid and benzoic acid. Powders containing 1% of transition metals, which Cr, Co, Cu, Fe, Mo, W and V, were used. According to study, TiO_2 powders loaded with Co and Cu scarcely influenced the photocatalytic activity of the pure support for

methanoic acid degradation. Also, they claimed that pure TiO_2 sample showed to be the most photoactivity for ethanoic acid degradation. On the other hand, TiO_2 powders loaded V showed minumum activity. Benzoic acid, even if with a larger number of atoms of carbon, was mineralized after exposure time shorter than those of the two aliphatic acids (Paola et al. 2004). These results indicated that photoactivity of the TiO_2 loaded with different metals shows varieties for different organic acids.

El-Bahy et al. analyzed photodegradation activity of lanthanide/TiO_2 and pure TiO_2 samples by using direct blue organic dye for 30 min. and at 25 ºC. According to their results, Gd/TiO_2 showed the highest photocatalytic activity due to high surface area and pore volume and low band gap. Moreover, it was showed that the photocatalytic activities of lanthanide ions-doped titania nanoparticles increased with decreasing the band gap values. They investigated photocatalytic activity as a function of time by using Gd/TiO_2, having the highest photocatalytic activity. As a result, remained dye was completely oxidized within 40 min. The band gap plays a critical role in deciding the photocatalytic activity of photocatalysts. It was estimated by the diffuse reflectance absorption spectrum (El-Bahy et al. 2008).

Wang et al. investigated rate constants for MB decomposition with different amounts of Fe doped photocatalysts. An increase in Fe content from 0.005% to 0.01% significantly enhanced the degradation rate, which should be attributed to the shift in optical absorption threshold of catalysts into visible region (Wang et al. 2010).

Song et al. investigated the relationship between the calcination temperature and photocatalytic activity of the Fe-TiO_2 by the degradation of the methyl orange under sunlight. The optimum calcination temperature for the best catalytic activity was determined to be 500 °C in their study. It was denoted that, the original concentration of the methyl orange solution was 20 mg/L, and the degradation rate of methyl orange solution was about 93% as the system was placed under sunlight for 5 hours. When calcination temperature was below 500 °C, degradation rate of methyl orange was low due to its low crystallinity. When the temperature reached 500 °C, more Fe^{3+} dissolved in the lattice of crystallized TiO_2. The calcined sample with high surface area and higher crystallinity showed the maximum photocatalytic activity. Over 500 °C, photoactivity decreased, which may be attributed to the anatase-rutile phase transition in the sample and the growth of the grain size which increased the electron-holes recombination and decreased the specific surface area (Song et al. 2007).

Qui et al. also studied photoactivity of the pure and Fe doped TiO_2. They found that Fe^{3+}-TiO_2 showed higher photo catalytic activity for degradation of the nitrite than Ce^{4+}-doped TiO_2 photocatalysts with the same experimental conditions (Qui et al. 2007).

CHAPTER 3

MATERIALS AND METHODS

3.1. Materials

In this thesis, titanium dioxide photocatalysts and iron doped titanium dioxides were synthesized. In the synthesis of the catalysts, tetrabutyl ortotitanate (TBOT) (Aldrich) was used as a precursor for titanium dioxide. Ethanol (EtOH) and deionised water (DIW) were used as solvents and hydrochloric acid (HCl) was used as peptizer in the sol-gel method. .

Also, magnesium oxide was synthetized, magnesium nitrate hexahydrate (Fluka) was used as a precursor. Used chemicals are summarized in the Table 3.1.

Table 3.1. Properties of materials used in catalyst synthesis.

Material	**Chemical formula**	**Molecular Weight (g/mol)**	**Purity (%)**
Tetrabutyl ortotitanate	$C_{16}H_{36}O_4Ti$	340.36	97
Ethanol	CH_3CH_2OH	46.07	99.5
Hydrochloric acid	HCl	36.45	37
Iron chloride hexahydrate	$FeCl_3 \cdot 6H_2O$	270.30	
Magnesium nitrate hexahydrate	$Mg(NO_3)_2 \cdot 6H_2O$	256.41	98

3.2. Methods

In this thesis, the experiments could be categorized into 3 groups.

- Preparation of the TiO_2 Fe/TiO_2 photocatalysts materials
- Characterization of the photocatalysts materials
- Photocatalytic activity tests

3.2.1. Preparation of the TiO_2 and Fe/TiO_2 Photocatalysts

TiO_2 photocatalysts were synthesized by using a modified single step sol-gel method. Firstly, necessary amount of TBOT were dissolved in ethanol and stirred for ten minutes at room temperature. The same time, second solution was prepared by mixing HCl solution and DIW at the room temperature. Necessary amount of second solution was taken and added to the first solution. After that, resulting solution was stirred at room temperature until the gelation was observed. After the gelation, gel was calcined in air at different temperatures with heating rate of 10 ºC/min. for 3 hours. Lastly, the material obtained was ground and sieved below 200 mesh size. For synthesizing Fe/TiO_2 photocatalysts, Fe^{3+} ions doped to the synthesized TiO_2 sample by impregnation method. Then, these impregnated samples were dried for 24 hours at 120 ºC and calcined at 200 ºC for 2 h with a heating rate of 10 ºC/min.

The schematic diagram of sol-gel procedure is given in Figure 3.1.

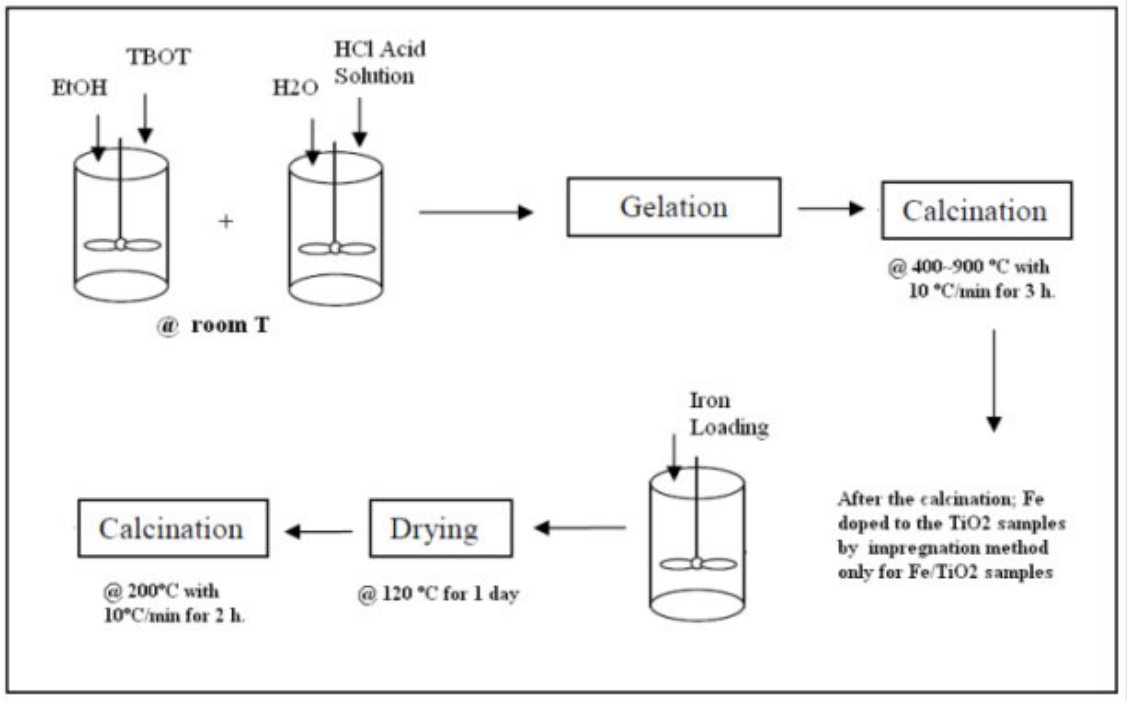

Figure 3.1. Experimental procedure for the preparation of titanium dioxide catalysts

3.2.2. Magnesium Oxide Preparation

Necessary amount of magnesium nitrate hexahydrate to obtain 2 gr of MgO was dissolved in DIW. MgO precipitated by adding ammonium hydroxide. When pH value of the solution reached 9-9.5 precipitation observed. Precipitated MgO was separated by a centrifuge. It was dried in the vacuum oven at 30 °C under the 100 mbar for 24 hrs. After that, dried precipitate was calcined at 600 °C for 24 hrs.

3.2.3. Characterization of the Photocatalysts

In the characterization of the samples, X-ray diffraction (XRD), UV/vis spectroscopy was used. XRD pattern of the samples were determined using a Philips Xpert XRA-480 Model X-ray diffractometer. Patterns were analyzed to find out the crystalline phase and also to calculate the average crystallite thickness using the Scherrer equation given below;

$$d = \frac{K\lambda}{\beta \cos\theta} \tag{3.1}$$

Where d is crystallite thickness, K is Scherrer constant (~0.9-1), λ is wavelength of the X-ray, β is the broadening of a diffracted peak at the full width at half maximum in terms of radian and θ is diffraction angle in degrees.

UV and visible spectrum of samples were obtained by using Perkin Elmer LAMBDA 45 UV/Vis Spectrophotometer with total diffuse reflectance collector. Diffuse reflectance spectrums of the samples were analyzed over a wavelength range of 250-800 nm. Diffuse reflectance (DR) is an excellent sampling tool for powders or crystalline materials. Pellets were used in the measurements and they were mounted in a blackened sample mask. $BaSO_4$ or MgO can be used as a reference material in the measurement of TiO_2 DR spectrum (Suzuki et al. 2005; Billmeyer 1969).

In this thesis, TiO_2 powders were pressed into pellets under the pressure of 5000 psi by using Camilla ’95 hydraulic press.

Figure 3.2. Picture of the Camilla ’95 Hydraulic Press

After that, DR spectrum was measured. Measured reflectance with the value of 100 (the reflectance expressed in the form of %). Diffuse reflectance UV/Vis spectra are shown in Figure 3.3.

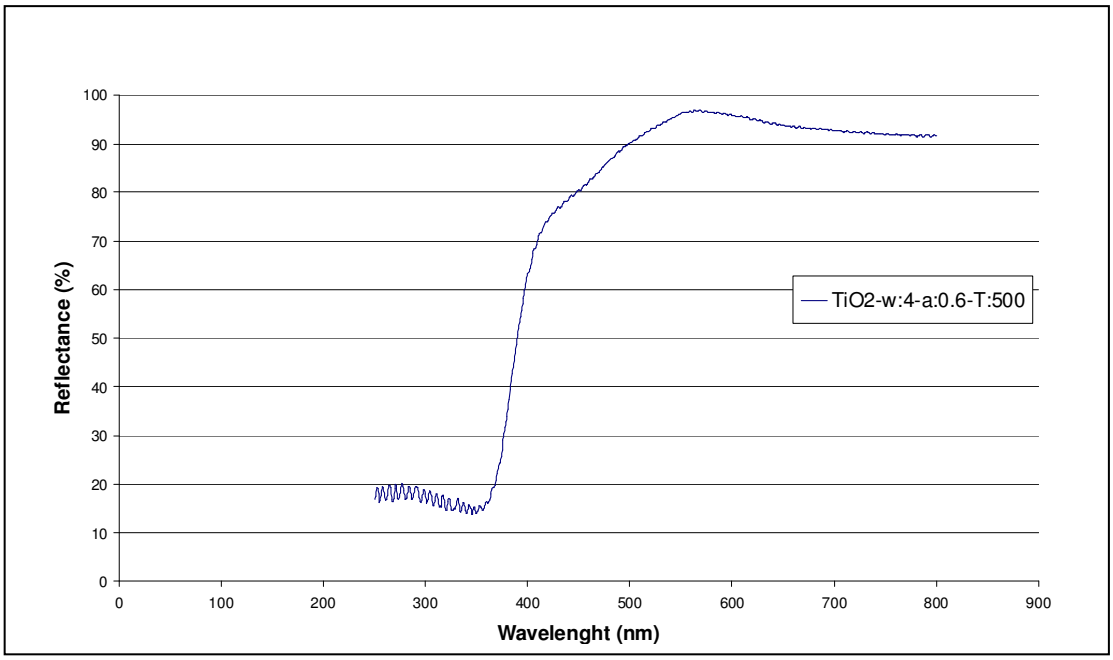

Figure 3.3. Diffuse Reflectance Spectra of TiO_2-w:4-a:0.6-T:500

The most useful analysis of diffuse reflectance data is provided by the theory of Kubelka Munk, which holds when the dimensions of the particles are comparable with, or smaller than, the wavelength of the incident light, and the diffuse reflection no longer allows one to separate the contribution of the reflection, refraction, and diffraction (i.e., scattering occurs) (Torrent and Barron 2002). Relationship between the reflectance % and wavelength is given by Kubelka Munk function;

$$K = \frac{(1-R)^2}{2R} \tag{3.2}$$

Where R is reflectance (%).

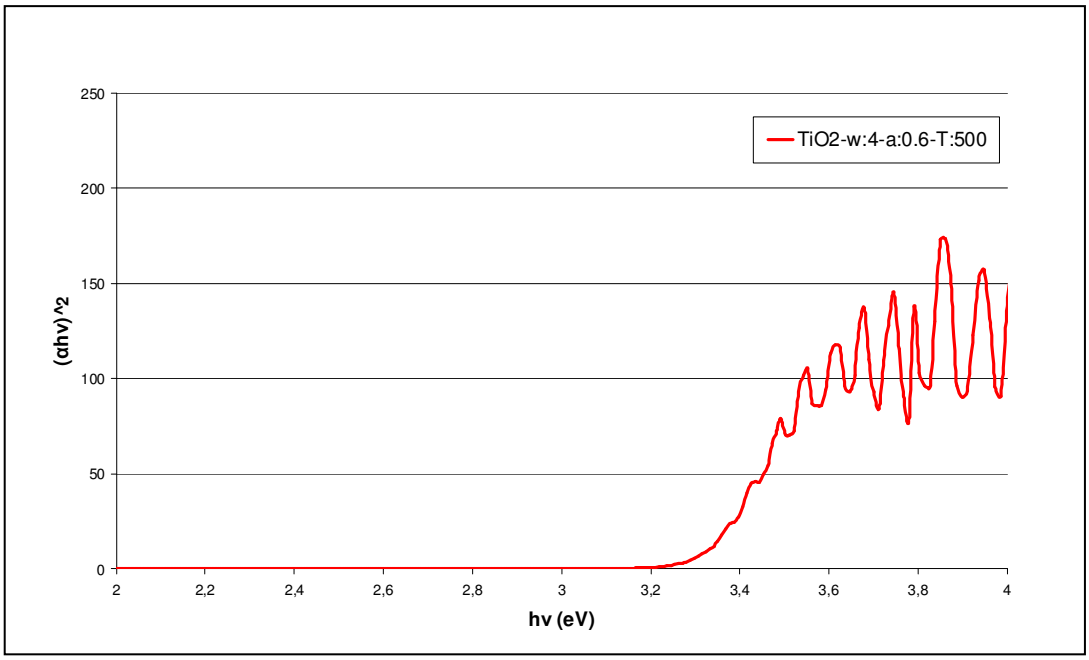

Figure 3.4. $(\alpha h\nu)^2$ versus hν plot for TiO_2-w:4-a:0.6-T:500

Then, direct band gap energy E_g can be finding in eV from the Equation (3.3) and indirect band gap can be find from the Equation (3.4). Also indirect band gap estimated according to determined according to $(\alpha h\nu)^{1/2}$ versus hν plot. A line is drawn tangential to intercept the linear part of the curve, as it seen in the Figure 3.5.

$$(K * h\nu)^2 = f(h * \nu) \tag{3.3}$$

$$(K * h\nu)^{\frac{1}{2}} = f(h * \nu) \tag{3.4}$$

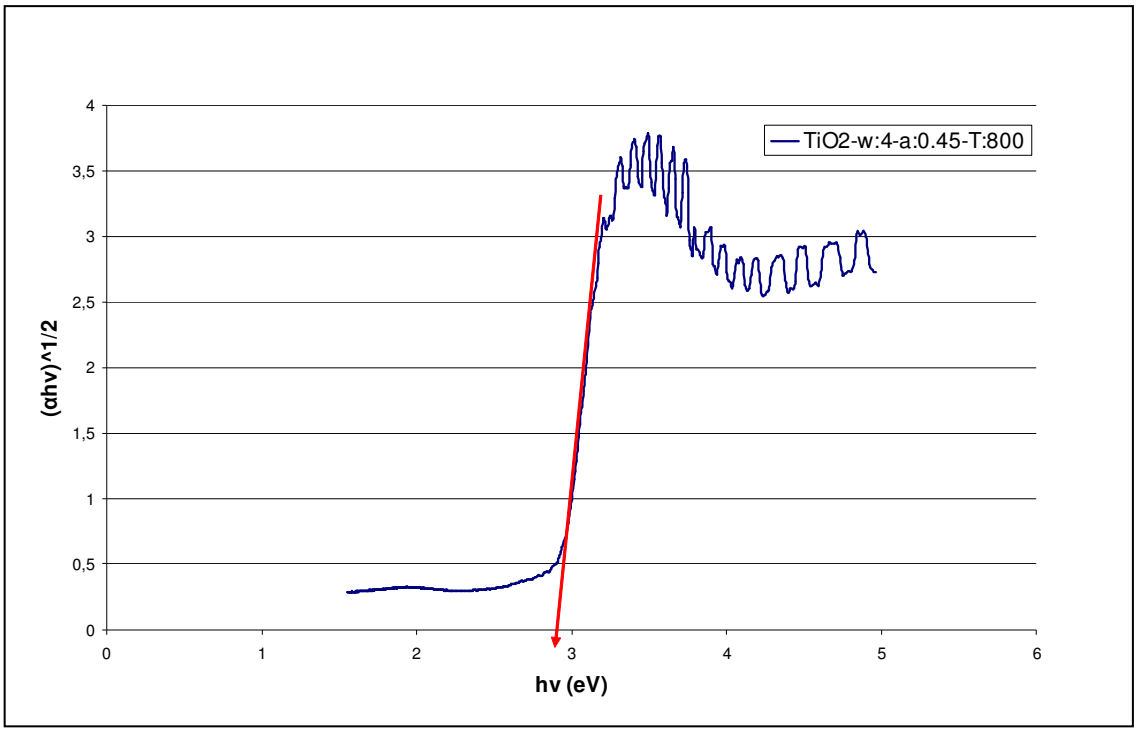

Figure 3.5. $(\alpha h\nu)^{1/2}$ versus hν plot for TiO_2-w:4-a:0.45-T:800

Spectra must generally be smoothed to calculate band gap energy. Various algorithms are available for this purpose. In this study, Polymath software was used. The intercept of the tangent to the plot will give a good estimation of the band gap energy for indirect and direct band gap materials.

3.2.4. Photocatalytic Activity Tests

To evaluate and compare the photocatalytic activity of TiO_2 and Fe doped TiO_2, photodegradation of methylene blue ($C_{16}H_{18}N_3S$) was performed under UV and fluorescence lamps on a home-made photoreactor system. Lamps were placed 15 cm away from the reactor. Under the experimental condition, initial MB concentration was equal to 10 ppm, light intensity was equal to about 10-11 kLux and TiO_2 dosage was kept at 20 g/L. Reaction time was 10 min for all synthesized TiO_2 and Fe doped TiO_2.

Typically, 0.2 g of TiO_2 or Fe doped TiO_2 photocatalysts were spread to the bottom of Petri dish as seen in Figure 3.6.

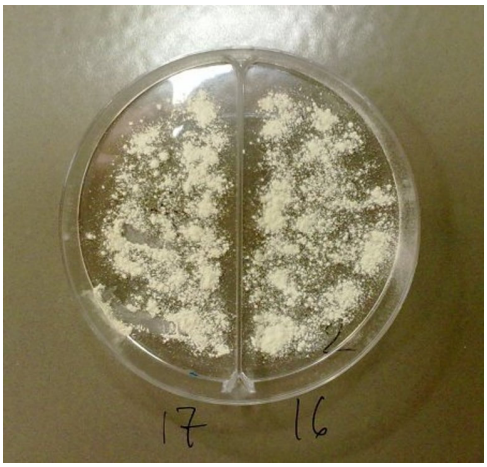

Figure 3.6. TiO_2 photocatalysts underlaid to the petri's dish.

MB aqueous solution (10 mL) was added onto the catalysts. Reaction was carried out for 10 min. System was cooled with ventilators. Reaction setup was seen in Figure 3.7.

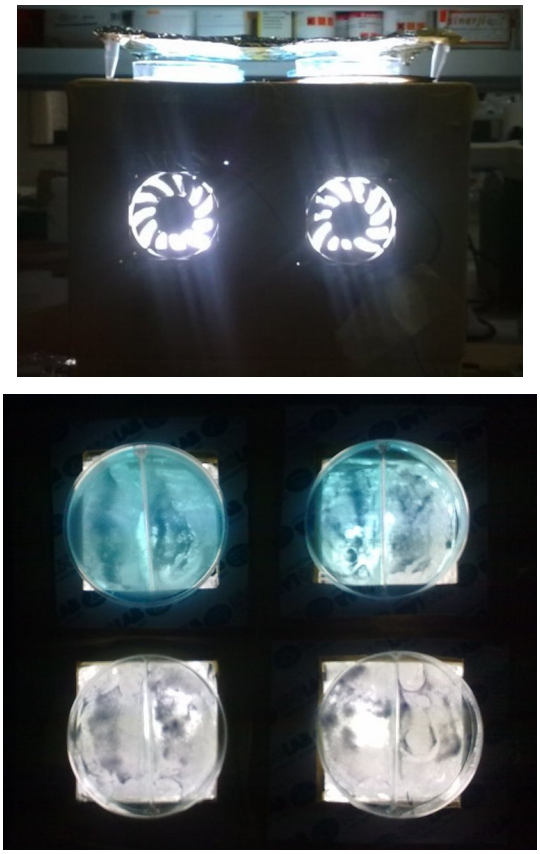

Figure 3.7. Photocatalytic activity tests setup

After the irradiation, the suspension was taken out and centrifuged at 2000 rpm for 4 min. Some of MB was taken from the top of the centrifuged sample into thevial. Then, it was centrifuged in the vial centrifuge at 7500 rpm for 5 min. UV-Vis spectroscopy was performed to measure the absorbance (A) of centrifuged samples at 664 nm.

The percent degradation of MB was calculated as follows (Zhang et al. 2011);

$$D = \frac{(A_0 - A)}{A_0} * 100\% \tag{3.5}$$

Where D is the percent degradation, A_0 is the absorbance of initial MB; A is the absorbance of the solution after illumination (Zhang et al. 2011). The measurement was repeated at three times for each photocatalysts drawn from one batch of material, and the each result was averaged.

CHAPTER 4

RESULTS AND DISCUSSION

4.1. Characteristics of TiO_2 and Fe Doped TiO_2 Photocatalysts

In this thesis, various TiO_2 and Fe doped TiO_2 photocatalysts were prepared to study their photocatalytic activity in the degradation of methylene blue. Prior to the photocatalytic activity, photocatalysts were characterized using X-Ray Diffraction (XRD) and Diffuse Reflectance Spectroscopy (DRS) to determine the crystalline phases, crystallite size and the band gap energy.

4.1.1. Crystalline Phase and Size of Pure TiO_2 and Fe Doped TiO_2 Photocatalysts

The crystalline phases present in the photocatalysts were identified by X-Ray diffraction method. In Figures 4.1, 4.2 and 4.3, the XRD spectra are shown as a function of the calcination temperatures of 400 ºC, 500 ºC and 600 ºC.

The sample prepared using H_2O/Ti of 4, HCl/Ti of 0.6 and 400 ^oC of calcination temperature (denoted as TiO_2-w:4-a:0.6-T:400) was repeated twice and it was found that XRD patterns of two samples showed the same pattern as seen in the Figure 4.1; hence, indicating a high repeatability of the experimental procedure used in this study. The strongest peak of the samples appears at 25.3º of 2-theta angle and also, the peak at this diffraction angle got sharper as the calcination temperature increased; hence indicating the increase of crystallite size. The crystalline phase of all of the TiO_2 calcined at 400 ºC, 500 ºC and 600 ºC for 3 h were anatase as seen in Figure 4.1.

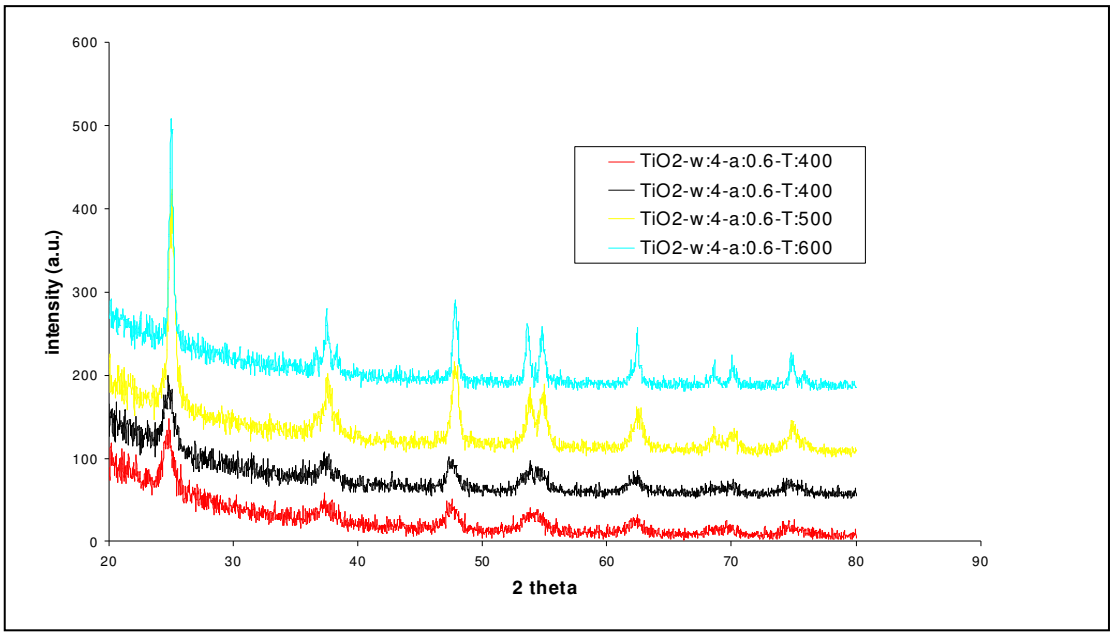

Figure 4.1. XRD patterns of TiO_2 photocatalysts as a function of calcinations temperatures of 400 ºC, 500 ºC and 600 ºC.

Figure 4.2 shows that for HCl/Ti ratio of 0.15, when the calcination temperature was 700 °C, rutile phase with a diffraction peak located at the 27.5º started to appear. At 800 °C, the peak at the 27.5º got sharper, but still, anatase phase was present. However, at 900 ºC, only rutile phase was observed.

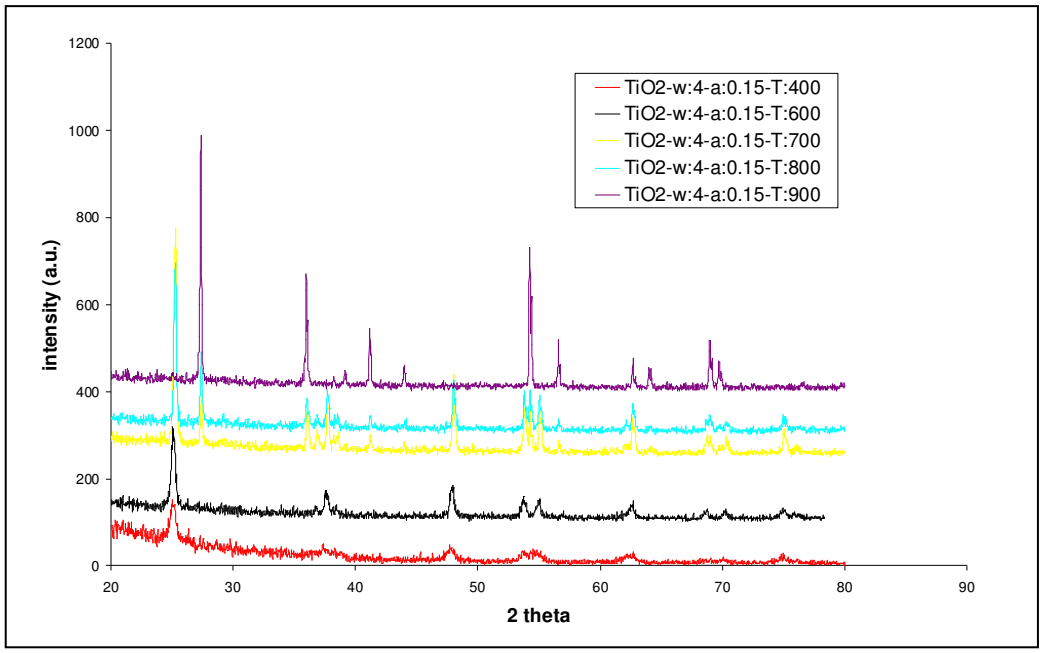

Figure 4.2. XRD patterns of TiO_2 photocatalysts as a function of calcination temperatures of 400 ºC, 600 ºC, 700 ºC, 800 ºC and 900 ºC for HCl/Ti ratio was 0.15.

Similarly, as seen in Figure 4.3 for HCl/Ti ratio of 0.45, when the calcination temperature was 800 °C, both rutile and anatase phases were present. The peak corresponding to rutile phase observed at 27.5º was higher than the anatase peak. At 900 ºC, only rutile phase was present based on the XRD measurements.

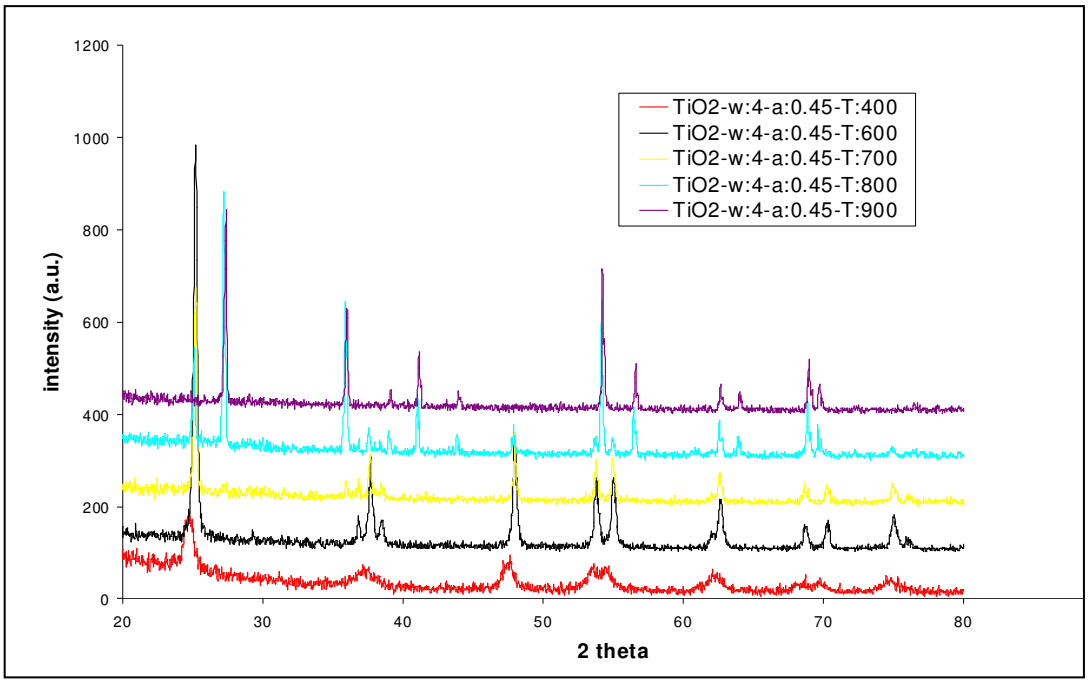

Figure 4.3. XRD patterns of TiO_2 photocatalysts as a function of calcination temperature of 400 ºC, 600 ºC, 700 ºC, 800 ºC and 900 ºC for HCl/Ti ratio was 0.45.

Figure 4.4 shows the effect of water used in the sol-gel method on the crystallite size and the crystalline phase formation at a constant calcination temperature of 500 ^{o}C. It was found that amount of water did not have any effect on the type of crystalline phase; in fact, only anatase phase formed. However, the water amount affected the crystallite size in such a way that as the water amount used in the sol-gel method decreased, the XRD peaks became sharper; indicating the increase of crystallite size.

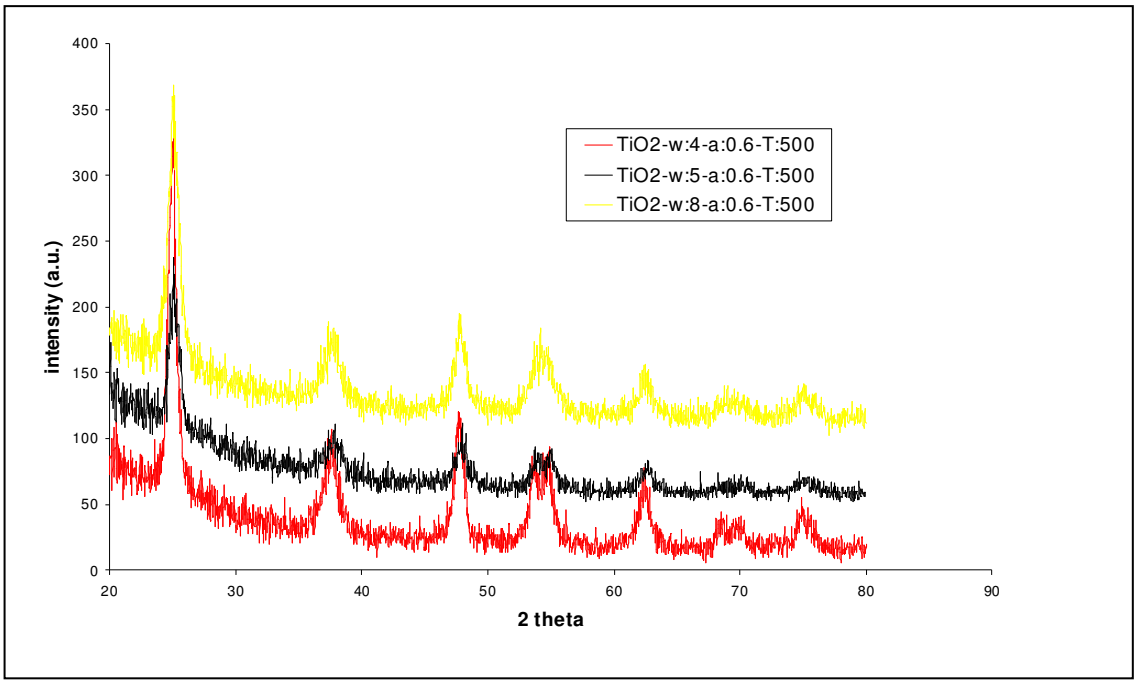

Figure 4.4. XRD pattern of TiO_2 photocatalysts as a function of water percentage in the TiO_2

The effect of hydrochloric acid amount used in the sol-gel method was investigated as well and shown in Figure 4.5. It was found that among all the HCl/Ti ratios, 0.3 HCl/Ti ratio gave the smallest crystallite size, ~12.9 nm, whereas HCl/Ti ratio did not affect the type of crystalline phase; in fact, anatase was the only crystalline phase.

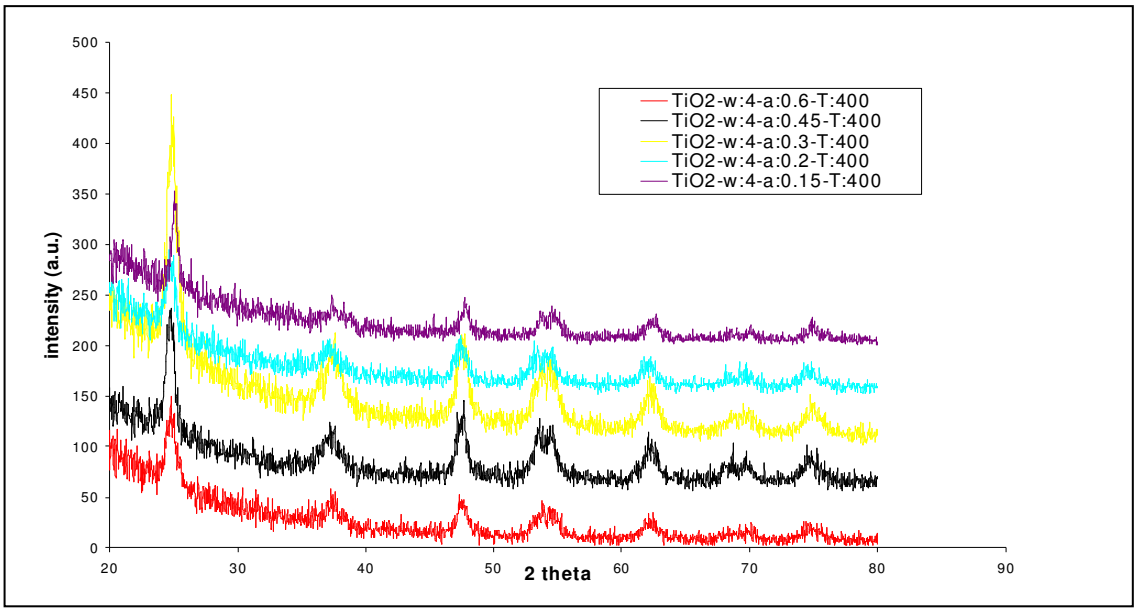

Figure 4.5. XRD patterns of TiO_2 photocatalysts as a function of HCl percentage in the TiO_2

The effect of Fe^{3+} doping on the phase formation was investigated at constant calcination temperatures. XRD patterns of all the samples are given in the Appendix A. Figures 4.6, 4.7 and 4.8 show the XRD patterns of different amounts of Fe^{3+} doped TiO_2 as a function of HCl/Ti ratios and the calcination temperatures. As seen in the figures, there is no characteristic peak corresponding to iron oxides for all iron loadings; hence, indicating that the crystallite size of iron oxides is less than 5 nm since it is known that XRD is sensitive to crystallite sizes larger than 5 nm. Besides, Fe^{3+} doping did not affect the type of crystalline phase formation. However, high Fe^{3+} loading, such as 1%, increased the crystallite size of TiO_2 whereas low loading, 0.1%, caused smaller crystallite sizes as compared to undoped TiO_2 as seen in Figure 4.6. Figures 4.7 and 4.8 show the effects of the calcination temperatures on the crystallite size and phases for 0.1% Fe loading. In fact, the crystallite size of TiO_2 increased with the calcination temperatures for 0.1% Fe loading and also, as compared to undoped TiO_2 at the same calcination temperatures, 0.1% Fe loading resulted in larger crystallites size.

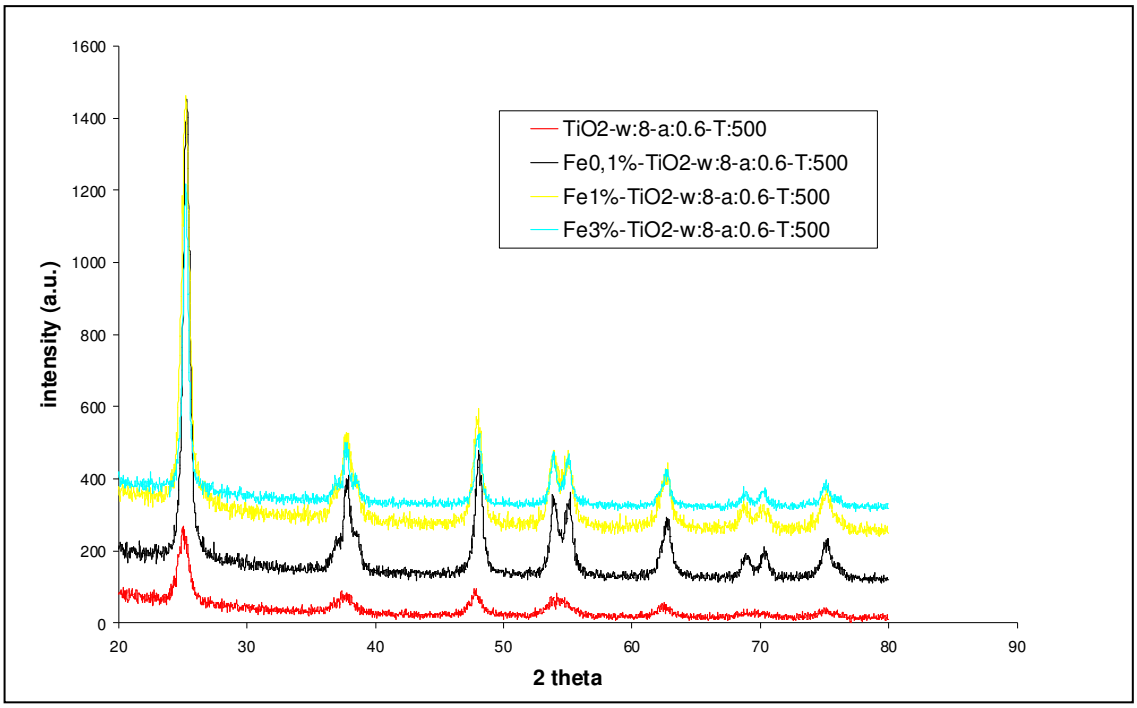

Figure 4.6. XRD patterns of pure and 0.1 w.%, 1 w.% and 3 w.% Fe^{3+} doped TiO_2-w:8 a:0.6-T:500 photocatalysts

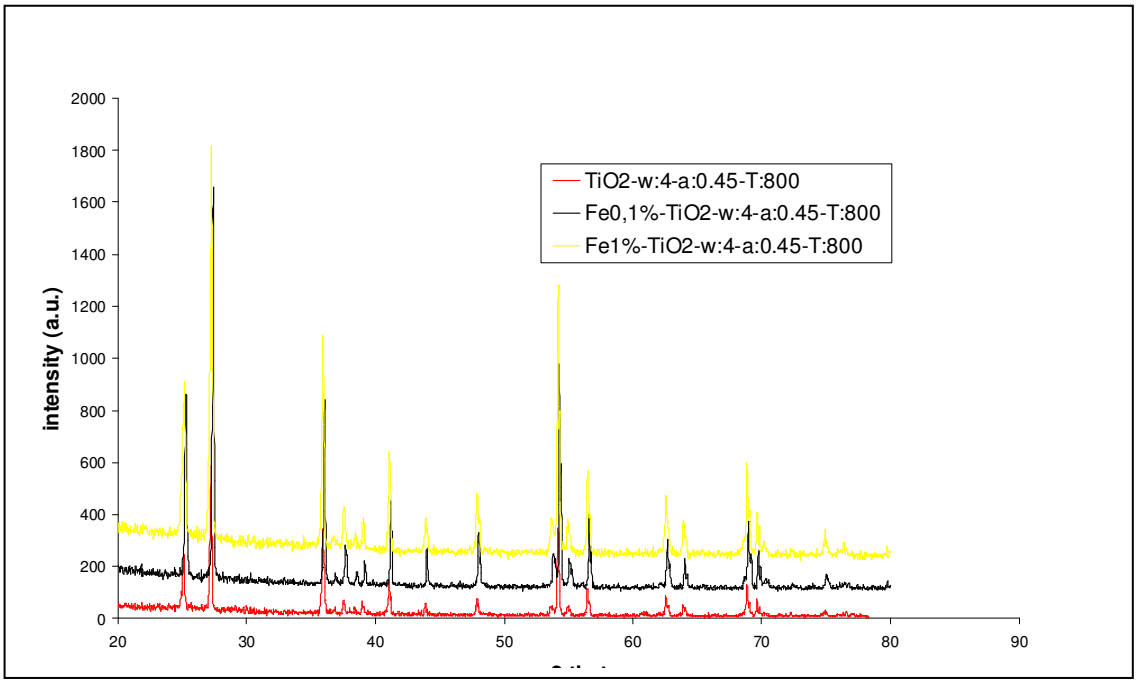

Figure 4.7. XRD patterns of pure and 0.1 w.% and 1 w.% Fe^{3+} doped TiO_2-w:4-a:0.45 T:800 photocatalysts

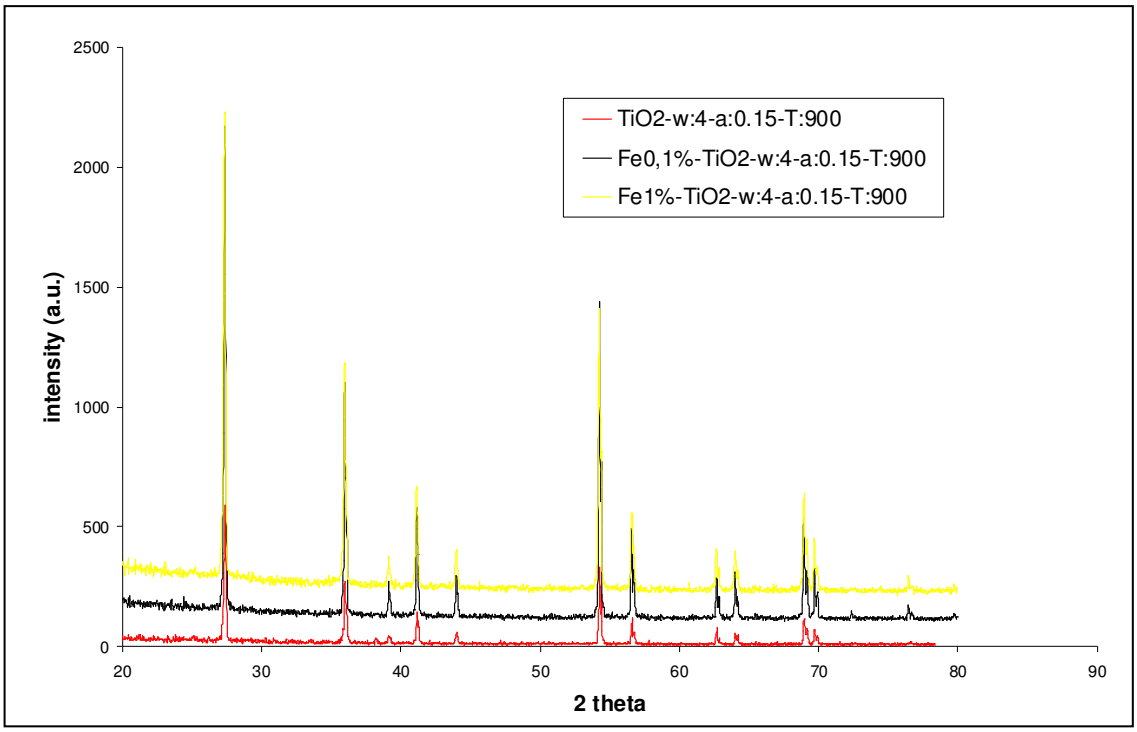

Figure 4.8. XRD patterns of pure and 0.1 w.% and 1 w.% Fe^{3+} doped TiO_2-w:4-a:0.15 T:900 photocatalysts

The crystallite size of TiO_2 and Fe^{3+} doped TiO_2 were calculated from the line broadening of corresponding X-ray diffraction peak using the Equation (3.1) (Scherrer equation) and are given in Table A.1 in Appendix A.

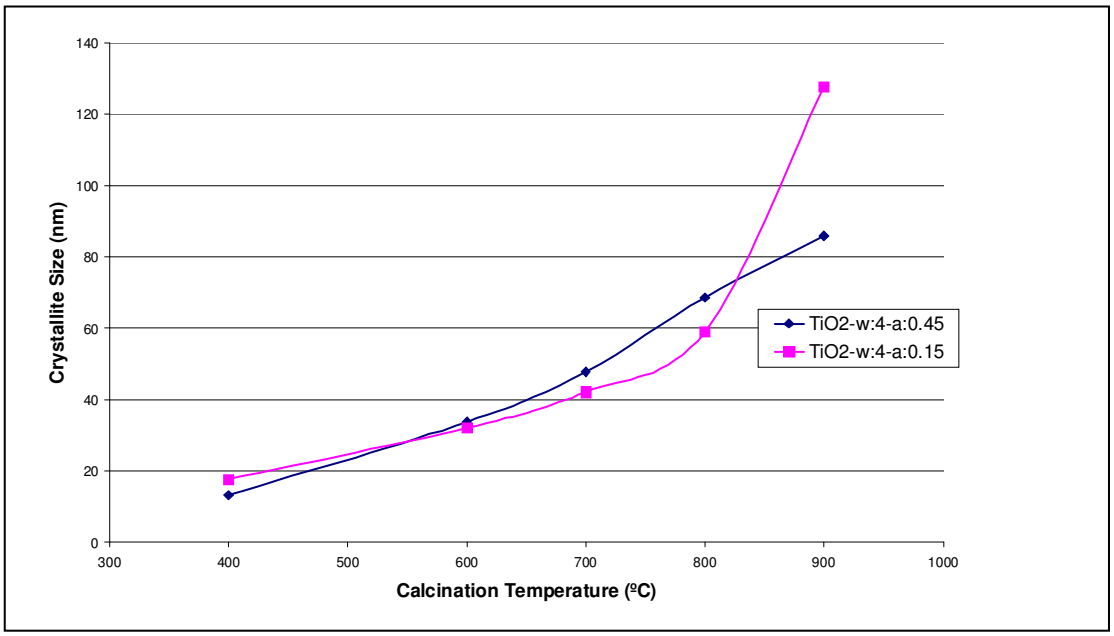

Figure 4.9. Effects of calcination temperature on the crystallite size

Figure 4.9 shows the effect of the calcination temperature on the average crystallite size of TiO_2 for two HCl/Ti ratios. Regardless of acid ratio, the crystallite size increased with the calcination temperature. At 0.45 of acid ratio, the crystallite sizes calculated for 700 and 800 ^oC are larger than that obtained with 0.15 of acid ratio. This may be due to the gel structure obtained during the synthesis; hence, resulting in different sintering behavior during the calcination.

Also, the amount of water used in the synthesis was changed at constant acid ratio and the calcination temperature. The effect of water amount on the crystallite size is shown in Figure 4.10. As seen in the figure, as the amount of water is increased, the crystallite size of TiO_2 decreased at both acid ratios and the calcination temperature.

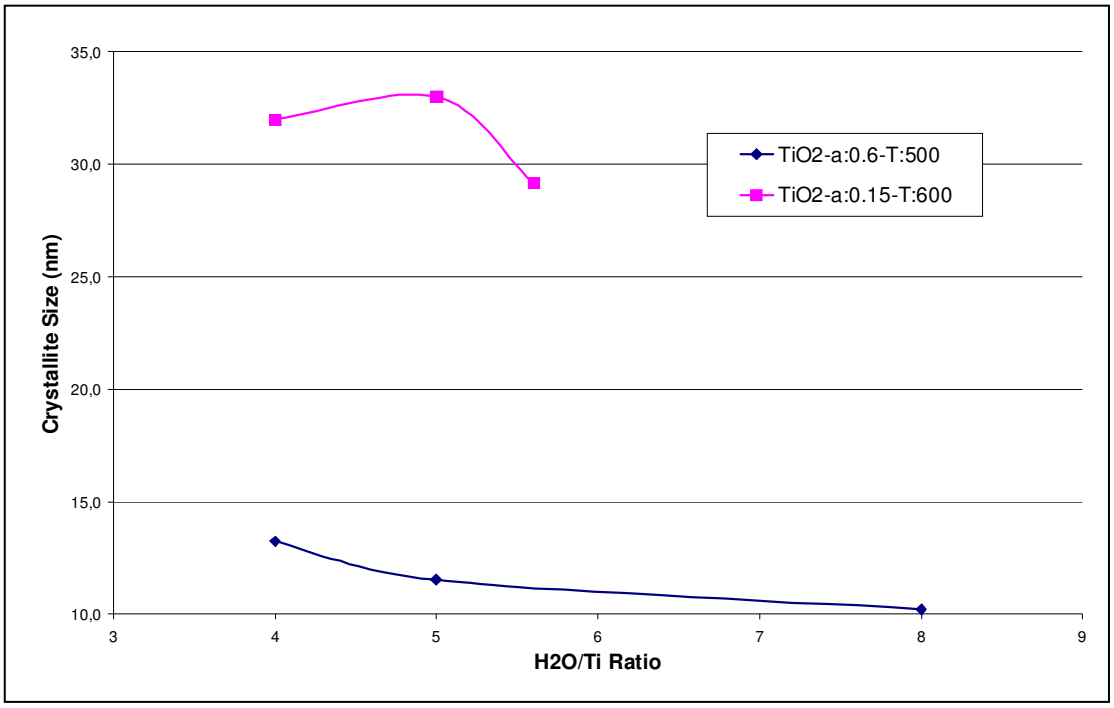

Figure 4.10. Effects of water amount in the TiO_2 on the crystallite size

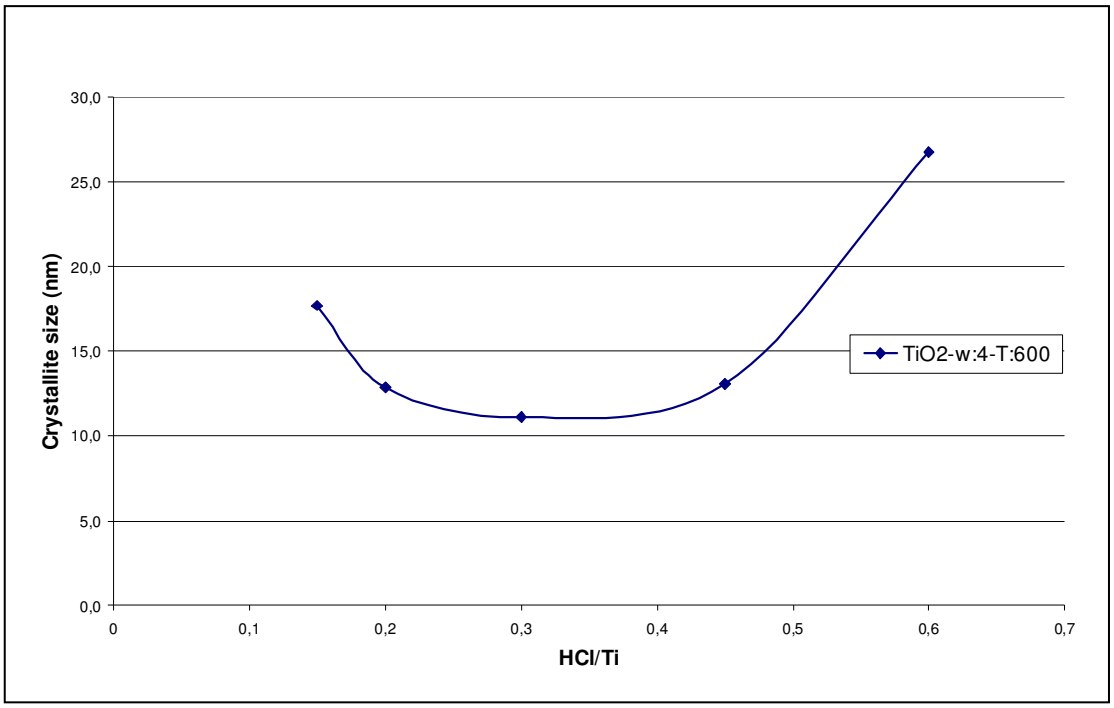

Figure 4.11. Effects of acid amount in the TiO_2 on the crystallite size

In contrast to the effect of water on the crystallite size, as HCl/Ti ratio is increased, the crystallite size decreases ~45% but when HCl/Ti ratio is 0.6, the crystallite size increases ~3 times that of the photocatalyst obtained at 0.3 of acid ratio. It is known that as the acid amount is increased, gelation slows and polymeric gel structure is obtained. This gel network may be the reason to ease the sintering effect on TiO_2; i.e. slowing down the increase of the crystallite size.

4.1.2. Band Gap Energies of TiO_2 and Fe Doped TiO_2 Photocatalysts

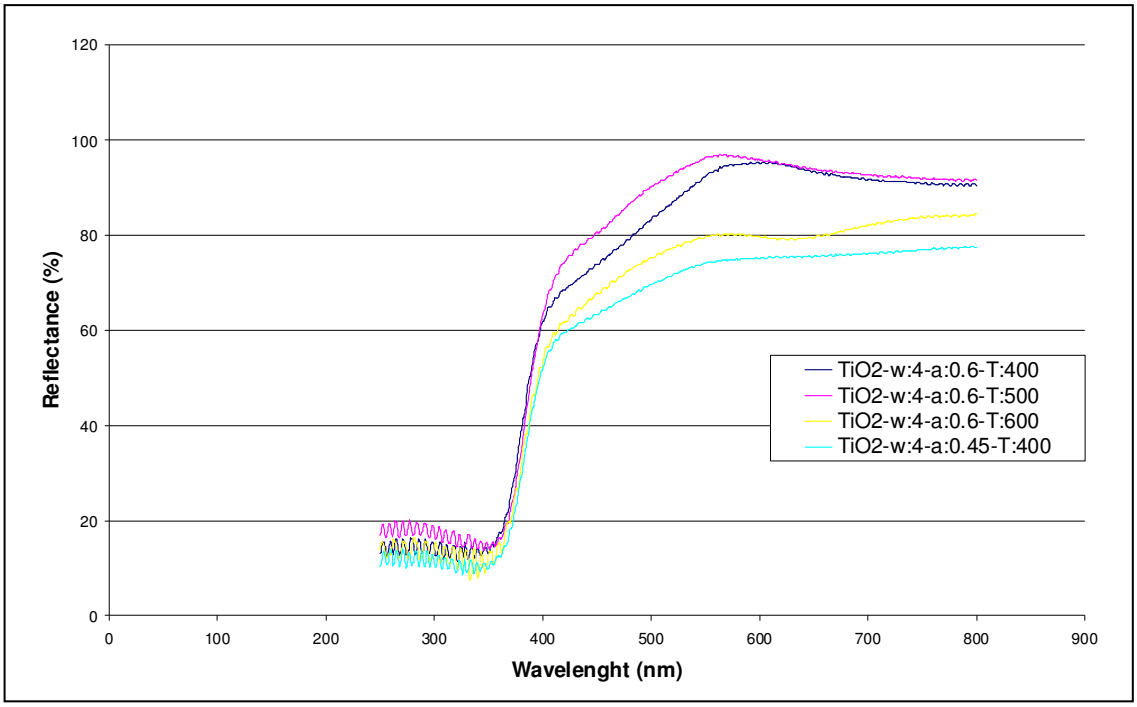

Figure 4.12. Diffuse reflectance spectra of TiO_2 as a function of acid ratio and the calcination temperatures

Figure 4.12 shows the diffuse reflectance spectra for various TiO_2 samples. The spectra were recorded at 1 nm intervals and the reflectance increases as the wavelength increases from blue (450 nm) to red (650 nm) region. Diffuse reflectance of all the TiO_2 and Fe doped TiO_2 pellet samples were measured over a wavelength range of 250-800 nm. diffuse reflectance spectra of all the synthesized samples are given in the Appendix.

Band gap energies of the TiO_2 samples were calculated from the Kubelka-Munk function using curve fit feature of the Polymath software.

Table 4.1. Direct band gap energies of TiO_2 samples

Pure TiO_2 catalysts	Direct Eg (eV)	Pure TiO_2 catalysts	Direct Eg (eV)
TiO2-w:4-a:0.6-T:400	3.336	TiO2-w:4-a:0.45-T:600	3.267
TiO2-w:4-a:0.6-T:500	3.308	TiO2-w:4-a:0.15-T:600	3.134
TiO2-w:4-a:0.6-T:600	3.357	TiO2-w:5.6-a:0.15-T:600	3.291
TiO2-w:4-a:0.45-T:400	3.319	TiO2-w:5-a:0.15-T:600	3.241
TiO2-w:4-a:0.6-T:500	3.309	TiO2-w:4-a:0.45-T:700	3.202
TiO2-w:5-a:0.6-T:500	3.301	TiO2-w:4-a:0.45-T:800	3.094
TiO2-w:8-a:0.6-T:500	3.324	TiO2-w:4-a:0.45-T:900	3.092
TiO2-w:4-a:0.3-T:400	3.280	TiO2-w:4-a:0.15-T:700	3.226
TiO2-w:4-a:0.2-T:400	3.252	TiO2-w:4-a:0.15-T:800	3.019
TiO2-w:4-a:0.15-T:400	3.284	TiO2-w:4-a:0.15-T:900	3.040

Table 4.2. Direct band gap energies of Fe^{3+} doped TiO_2 samples

0.1 w.% Fe doped TiO_2 catalysts	Direct Eg (eV)	1 w.% Fe doped TiO_2 catalysts	Direct Eg (eV)
Fe0.1%-TiO2-w:4-a:0.6-T:400	3.212	Fe1%-TiO2-w:4-a:0.6-T:400	2.932
Fe0.1%-TiO2-w:4-a:0.6-T:500	3.205	Fe1%-TiO2-w:4-a:0.6-T:500	2.915
Fe0.1%-TiO2-w:4-a:0.6-T:600	3.110	Fe1%-TiO2-w:4-a:0.6-T:600	2.912
Fe0.1%-TiO2-w:4-a:0.45-T:400	3.200	Fe1%-TiO2-w:4-a:0.45-T:400	2.718
Fe0.1%-TiO2-w:8-a:0.6-T:500	3.226	Fe1%-TiO2-w:8-a:0.6-T:500	2.548
Fe0.1%-TiO2-w:4-a:0.45-T:600	3.132	Fe1%-TiO2-w:4-a:0.45-T:600	2.887
Fe0.1%-TiO2-w:4-a:0.15-T:600	3.173	Fe1%--TiO2-w:4-a:0.15-T:600	2.920
Fe0.1%-TiO2-w:5.6-a:0.15-T:600	3.089	Fe1%--TiO2-w:5.6-a:0.15-T:600	3.050
Fe0.1%-TiO2-w:4-a:0.45-T:700	3.136	Fe1%-TiO2-w:4-a:0.45-T:700	3.101
Fe0.1%-TiO2-w:4-a:0.45-T:800	3.048	Fe1%-TiO2-w:4-a:0.45-T:800	2.947
Fe0.1%-TiO2-w:4-a:0.45-T:900	3.021	Fe1%-TiO2-w:4-a:0.45-T:900	2.964
Fe0.1%-TiO2-w:4-a:0.15-T:700	3.091	Fe1%-TiO2-w:4-a:0.15-T:700	2.956
Fe0.1%-TiO2-w:4-a:0.15-T:800	3.017	Fe1%-TiO2-w:4-a:0.15-T:800	2.976
Fe0.1%-TiO2-w:4-a:0.15-T:900	3.052	Fe1%-TiO2-w:4-a:0.15-T:900	2.970

Calculated direct band gap energies of the TiO_2 and Fe^{3+} doped TiO_2 samples are given in the Table 4.1 and Table 4.2, respectively. Indirect band gap energies of the selected TiO_2 samples were also calculated and found that indirect band gap energies are smaller than that of direct band gap energies for the same samples as seen Table 4.3.

Table 4.3. Indirect band gap energies of TiO_2 samples

Fe^{3+} doped TiO_2 catalysts	Indirect Eg (eV)
TiO2-w:4-a:0.45-T:800	2.837
TiO2-w:4-a:0.45-T:900	2.824
TiO2-w:4-a:0.15-T:800	2.883
TiO2-w:4-a:0.15-T:900	2.877

4.2. Photocatalytic Degradation of Methylene Blue (MB) on TiO_2

The photoactivities of TiO_2 samples in the decomposition of MB under visible light illumination were determined following the procedure given in Chapter 3.

Figure 4.13 shows the effect of the calcination temperature on the photocatalytic degradation activity of TiO_2 synthesized under constant sol-gel parameters: H_2O/Ti=4 and HCl/Ti=0.6. It was found that as the calcination temperature increases, the MB degradation increases. For instance, the photocatalytic degradation of TiO_2-w:4-a:0.6-T:400, TiO_2-w:4-a:0.6-T:500 and TiO_2-w:4-a:0.6-T:600 were 2.37%, 6.90% and 9.11%, respectively, when the reaction time was 10 min.

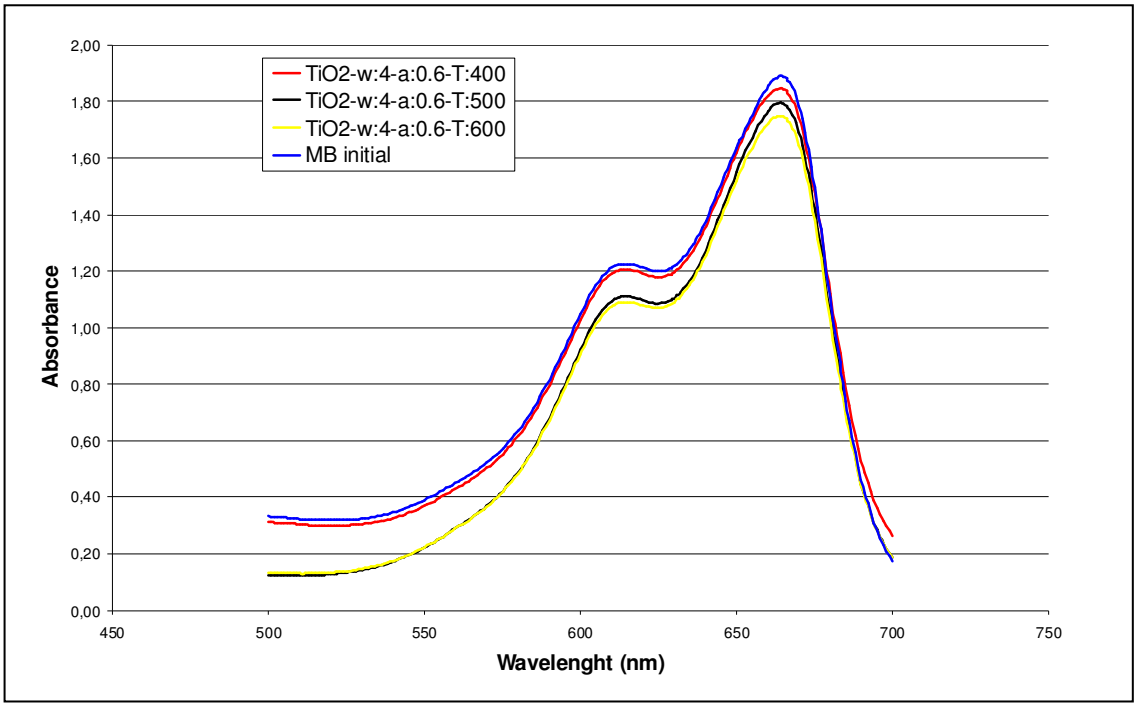

Figure 4.13. UV/Vis Absorbance Spectra of TiO_2-w:4-a:0.6-T:400, TiO_2-w:4-a:0.6-T:500 and TiO_2-w:4-a:0.6-T:600 after the illumination

Similarly, as seen in Figure 4.14, TiO_2 calcined at 800 and 900 ^oC were more active than TiO_2 calcined at 400-700 ^oC. In fact, the photocatalytic degradation of TiO_2-w:4-a:0.45-T:400, TiO_2-w:4-a:0.45-T:600, TiO_2-w:4-a:0.45-T:700, TiO_2-w:4-a:0.45-T:800 and TiO_2-w:4-a:0.45-T:900 were 5.66%, 7.78%, 11.93%, 21.81% and 25.00%, respectively, in 10 min of the reaction. It was found that TiO_2-w:4-a:0.45-T:900 sample showed the maximum photocatalytic activity and for comparison, Degussa (P25) TiO_2 was used under the same reaction conditions and the degradation of MB on Degussa TiO_2 was 30.54% in 10 min. Also, to check if the degradation is solely due to photocatalysis, the same experiments were carried out in the dark and there was no degradation or adsorption of MB on TiO_2 samples.

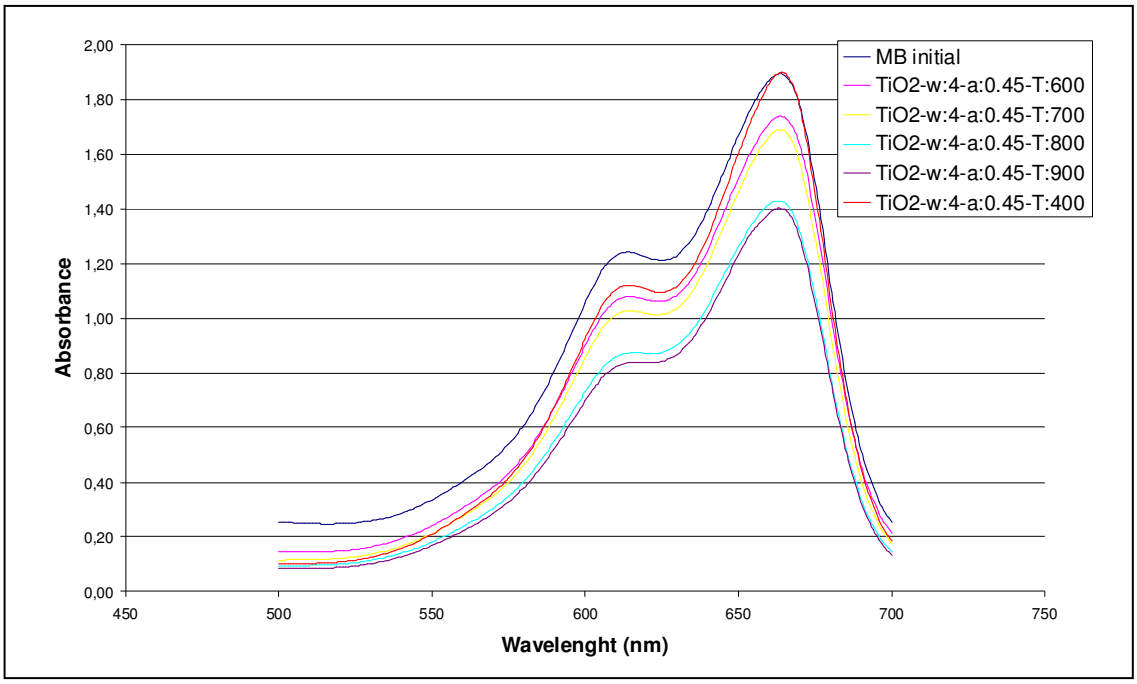

Figure 4.14. UV/Vis Absorbance Spectra of TiO_2-w:4-a:0.45-T:400, TiO_2-w:4-a:0.45 T:600, TiO_2-w:4-a:0.45-T:700, TiO_2-w:4-a:0.45-T:800 and TiO_2-w:4-a:0.45 T:900 after the illumination

The reason behind the variation observed in degradation activity results could be explained by crystallite sizes and band gap energies since it is known that the type of crystalline phase, crystallite size and band gap energy are the main factors influencing photocatalytic activity. Table 4.4 summarizes the MB degradation obtained in 10 min for TiO_2 samples (with H_2O/Ti=4 and HCl/Ti=0.15) calcined at 400-900 ºC and also the corresponding spectra are shown in Figure 4.15. As seen in the Table, the degradation

activity increases with the calcination temperature. This could not directly be correlated with the band gap energies since TiO_2-w:4-a:0.15-T:400 and TiO_2-w:4-a:0.15-T:700 has similar band gap energies but MB degradation on TiO_2-w:4-a:0.15-T:700 is 12% as compared to 0.11% obtained on TiO_2-w:4-a:0.15-T:400. The only difference is the crystalline phases present in the samples; for instance, TiO_2-w:4-a:0.15-T:700 contains both anatase and rutile phases whereas TiO_2-w:4-a:0.15-T:400 has only anatase phase. Also, the average anatase crystallite size of TiO_2-w:4-a:0.15-T:400 is ~18 nm and that of TiO_2-w:4-a:0.15-T:700 is ~44 nm. One may expect higher activity for small crystallite size sample but as seen in the Table, TiO_2-w:4-a:0.15-T:400 (with small crystallite size) is not active; giving only 0.11% degradation in 10 min. The difference in photocatalytic degradation could be explained by the presence of rutile phase in TiO_2-w:4-a:0.15-T:700. In fact, TiO_2-w:4-a:0.15-T:900 has only rutile phase and its photocatalytic activity is higher than that of TiO_2-w:4-a:0.15-T:700

Table 4.4. Photocatalytic efficiency compared to the crystallite sizes and direct band gap energies

Pure TiO_2 Samples	%Degradation of MB	Crystalline Phase	Crystallite size (nm)	Direct band gap (eV)
TiO2-w:4-a:0.15-T:400	0.11	Anatase	17.7	3.284
TiO2-w:4-a:0.15-T:600	10.80	Anatase	31.99	3.134
TiO2-w:4-a:0.15-T:700	12.00	Anatase/Rutile	44.36/120.34	3.226
TiO2-w:4-a:0.15-T:800	14.81	Anatase/Rutile	57.26/74.32	3.09
TiO2-w:4-a:0.15-T:900	19.03	Rutile	127.74	3.040

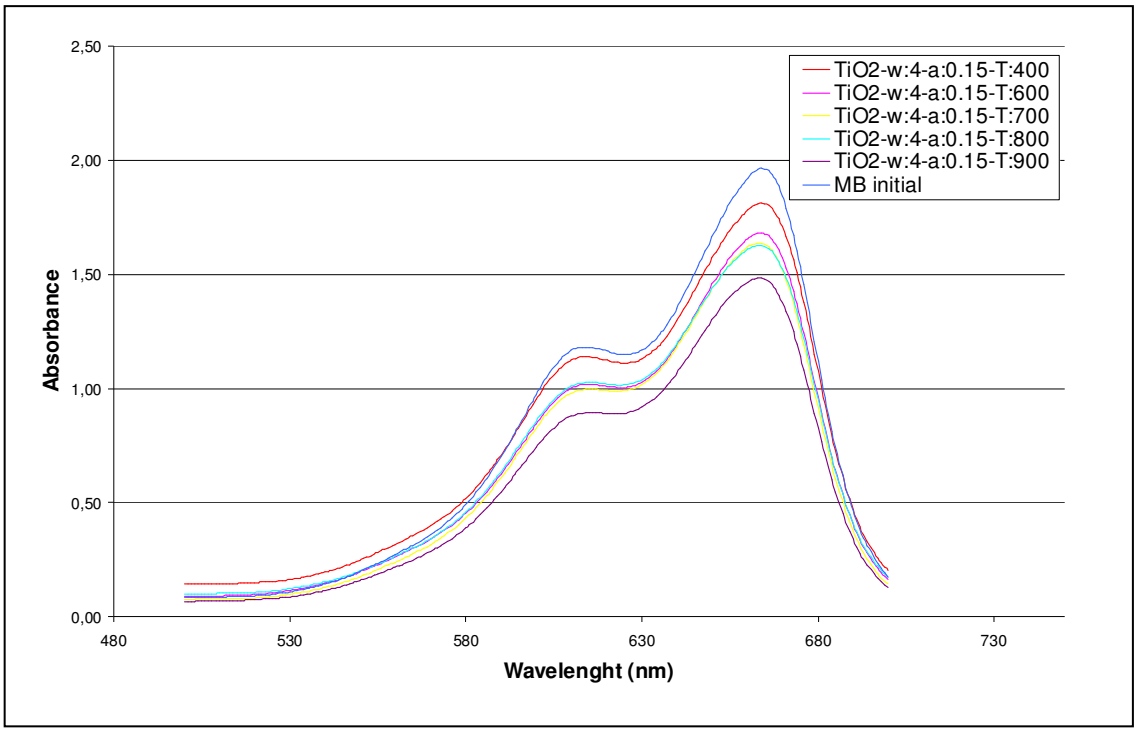

Figure 4.15. UV/Vis Absorbance Spectra of TiO_2-w:4-a:0.15-T:400, TiO_2-w:4-a:0.15 T:600, TiO_2-w:4-a:0.15-T:700, TiO_2-w:4-a:0.15-T:800 and TiO_2-w:4-a: 0.15-T:900 after the illumination

Photocatalytic activity of TiO_2-w:4-a:0.6-T:500, TiO_2-w:5-a:0.6-T:500 and TiO_2-w:8-a:0.6-T:500 were 4.42%, 1.82% and 0.57% respectively. The corresponding absorbance spectra of methylene blue before and after the reactions are shown in Figure 4.16. Increasing water amount used during the sol-gel preparation resulted in smaller crystallite size but water amount did not change the formation of type of crystalline phase; only anatase phase was present. Hence, it seems that the high MB degradation occurred on TiO_2 with large anatase crystallite size (TiO_2-w:4-a:0.6-T:500).

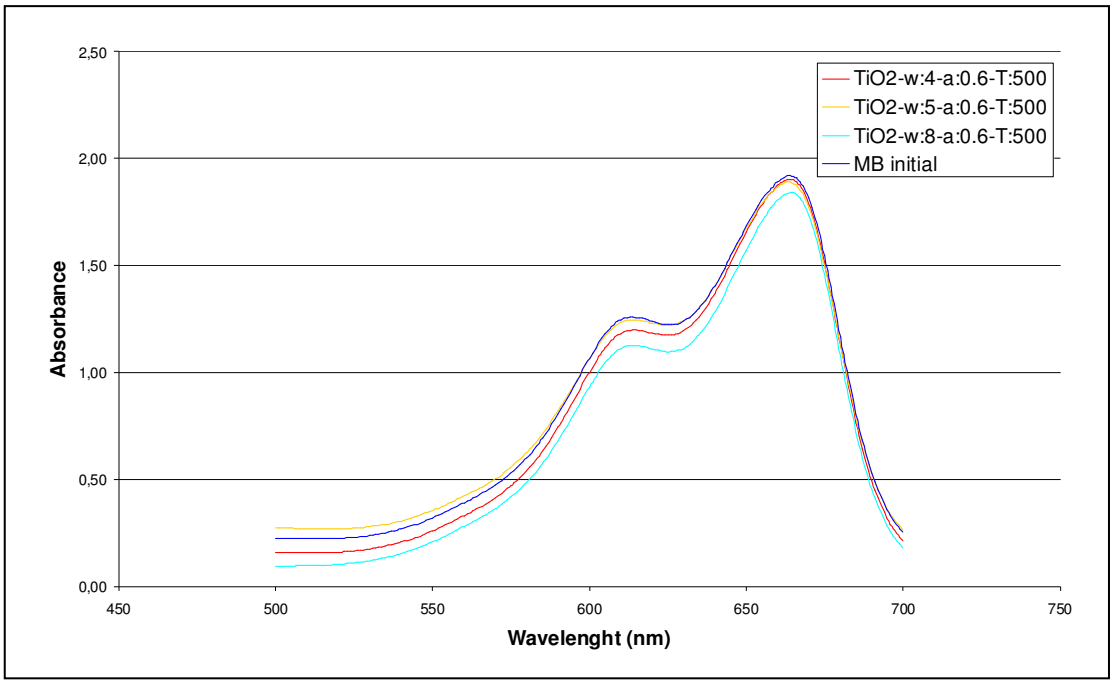

Figure 4.16. UV/Vis Absorbance Spectra of TiO_2-w:4-a:0.6-T:500, TiO_2-w:5-a:0.6-T:500 and TiO_2-w:8-a:0.6-T:500 after the illumination

Similarly, photocatalytic activity of TiO_2 as a function of HCl/Ti ratio at a constant calcination temperature of 400 ^oC is given in Figure 4.17. The photocatalytic degradation of MB on TiO_2-w:4-a:0.15-T:400, TiO_2-w:4-a:0.2-T:400, TiO_2-w:4-a:0.3-T:400, TiO_2-w:4-a:0.45-T:400 and TiO_2-w:4-a:0.6-T:400 were 2.37%, 5.66%, 1.09%, 0.70% and 0.11% respectively. It is seen that TiO_2-w:4-a:0.45-T:400 and TiO_2-w:4-a:0.2-T:400 have ~13 nm average crystallite size but the maximum degradation was obtained on TiO_2-w:4-a:0.45-T:400. Although the crystalline phase of all the TiO_2 photocatalysts are anatase and has similar band gap energies, TiO_2 prepared with HCl/Ti=0.45 is more active than the others. At this point, there is no clear explanation why there is significant difference in the degradation activities for similar crystallite size and phases. This may be due to the presence of strongly adsorbed chloride ions on TiO_2.

The effect of pH change on the absorbance of MB was checked acidifying the MB solution using HCl and HNO_3. When the pH of the MB was 2 at room temperature, the absorbance of MB did not chage. Therefore, the pH change (less than ~1 pH decrease) observed during the degradation reaction did not affect the absorbance measurements; i.e. there was no effect of pH change on the measurement of the MB concentration using the UV/Vis absorbance.

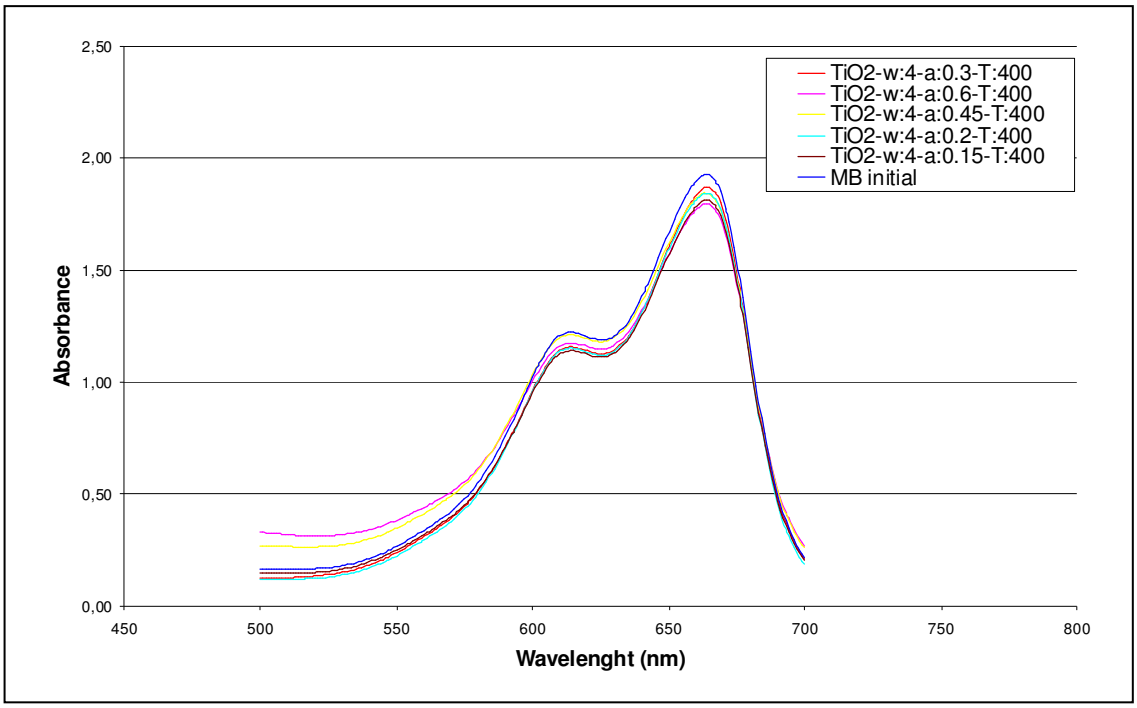

Figure 4.17. UV/Vis Absorbance Spectra of TiO_2-w:4-a:0.15-T:400, TiO_2-w:4-a:0.2 T:400, TiO_2-w:4-a:0.3-T:400, TiO_2-w:4-a:0.45-T:400 and TiO_2-w:4-a:0.6 T:400 after the illumination

The crystallite size of the TiO_2 samples determined from the line broadening of corresponding X-ray peaks by using the Scherrer equation. Red line in the Figure 4.18 shows the crystallite size versus calcination temperature for anatase phase and constant acid and water ratios samples. Crystallite sizes increased with the increase of calcination temperature. Blue line shows the degradation as a function of crystallite sizes. When crystallite sizes increasing photocatalytic degradation of methylene blue increased due to calcination temperature. Methylene blue degradation is the highest at the calcination temperature of 700 ºC. This figure clearly shows that the photocatalytic degradation activity of pure TiO_2 increases with the crystallite size when the crystalline phase is anatase and the acid ratio is 0.45.

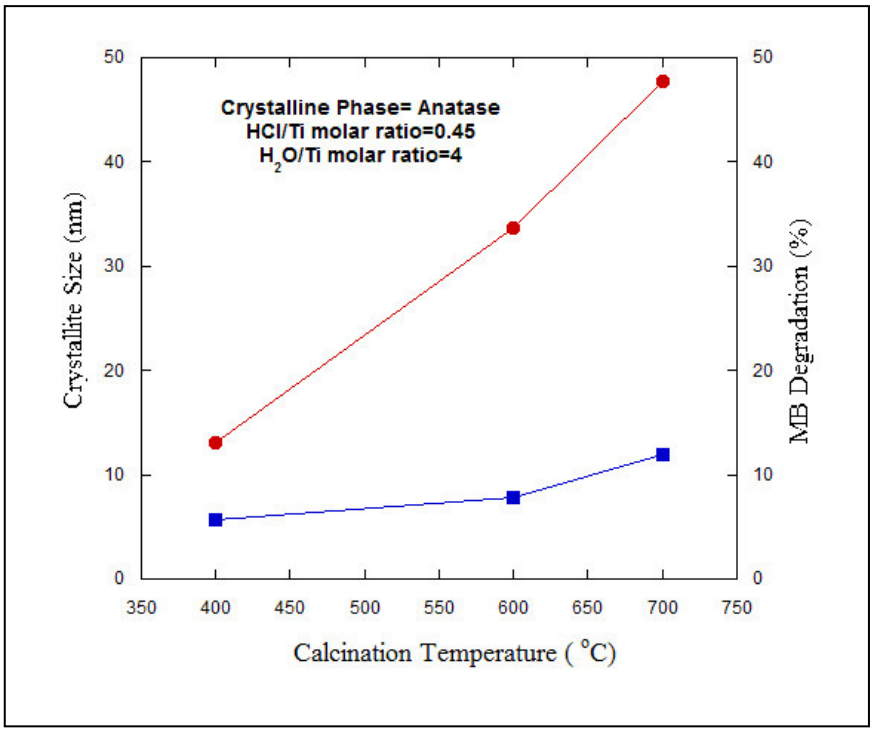

Figure 4.18. The effect of the crystallite size, calcination temperature on MB degradation for the sample of TiO2-w:4-a:0.45-T:400, TiO2-w:4 -a:0.45-T:600 and TiO2-w:4-a:0.45-T:700

In contrast to the acid ratio of 0.45, the appearance of rutile phase occurred at 700 °C when the acid ratio was 0.15 as seen in Table 4.4. Interestingly, MB degradation is the same for acid ratios, 0.45 and 0.15, at the same calcination temperature of 700 °C. The only difference is the presence of rutile phase. The crystallite size of anatase for the acid ratio of 0.15 and 0.45 is ~44 nm and 48 nm, respectively. This seems to indicate that the presence of rutile does not have any effect on the photodegradation of MB under these conditions. But this may be due to the large crystallite size of rutile which is 120 nm at 700 °C of calcination temperature and 0.15 of acid ratio. In terms of band gap energies, there is no significant difference as the acid ratio is increased from 0.15 to 0.45 at the constant calcination temperature of 700 °C. A Moreover, it was reported in the literature that small crystallite size had higher activities, but according to Table 4.4, TiO_2 calcined at 400 ºC which has the smallest crystallite size is not active. In fact, not only the crystallite size but also the acid ratio seems to affect the MB photocatalytic degradation activity. As seen in Figure 4.19, at constant 400 °C of the calcination temperature, the crystalline phase is anatase and as the acid ratio increases, the crystallite size decreases from ~18 nm to ~11 nm and the MB degradation first increases

to ~6% and then ~2% as the acid ratio increases. As seen in Figure 4.19, crystallite size does not significantly change after the acid of 0.3 but MB degradation shows a dome shape degradation versus acid ratio. This seems to indicate the effect of acid ratio which is not related to the crsytallite size for the same anatase crystalline phase.

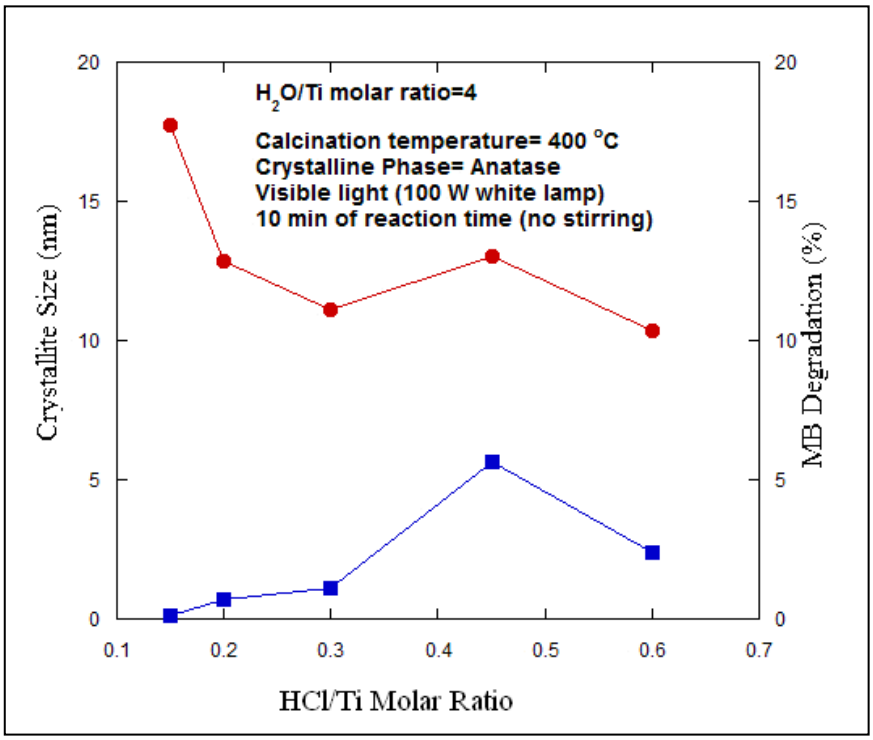

Figure 4.19. The effect of HCl/Ti molar ratio and on MB degradation for the sample of TiO_2-w:4-a:0.15-T:400, TiO_2-w:4-a:0.2-T:400, TiO_2-w:4-a:0.3-T:400, TiO_2-w:4-a:0.45-T:400 and TiO_2-w:4-a:0.6-T:400

Similar sol-gel preparation effect was also observed for water ratio. As seen in Figure 4.20, the acid ratio and the calcination temperature was kept at 0.15 and 600 ^oC. For all the water ratios, the crystalline phase was anatase and the crystallite size did not change with water ratio as seen in the figure. However, the highest MB photodegration, 10%, was obtained at water ratio of 4 as compared to ~6% degradation observed at water ratio of 6. Since the experimental error in this study was ~3% of the average values, the difference observed is significant. This cannot be solely explained by crystallite size nor band gap energies which did not change with water ratio as given in Table 4.5. Further detailed study on the pore size, pore size distribution and also the calculation of indirect band gap energies together with the controlled wavelength of

light source must be carried out to better understand the role of material properties and relationship to the sol-gel preparation parameters.

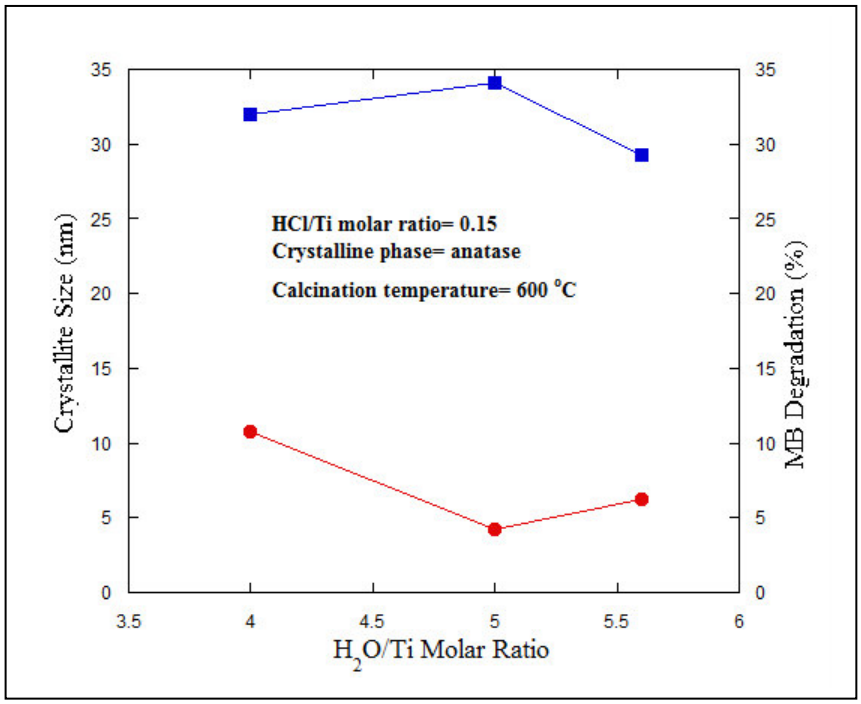

Figure 4.20. Relation between the crystallite size, H_2O/Ti molar ratio and MB % degradation for the sample of TiO_2-w:4-a:0.15-T:600, TiO_2-w:5-a 0.15-T:600 and TiO_2-w:5.6-a:0.15-T:600

Table 4.5. Band gap energies of TiO_2-w:4-a:0.15-T:600, TiO_2-w:5-a:0.15-T:600 and TiO_2-w:5.6-a:0.15-T:600

TiO_2 sample	**Band gap (eV)**
TiO_2-w:4-a:0.15-T:600	3.134
TiO_2-w:5-a:0.15-T:600	3.291
TiO_2-w:5.6-a:0.15-T:600	3.241

Figure 4.21 shows the effect of high calcination temperatures on crystallite sizes, crystalline phases and methylene blue degradation for the constant water and acid ratio of 4 and 0.15 of acid ratio. When calcination temperatures increasing rutile phases start to occur. Both anatase and rutile phases are present at 700 ºC and 800 ºC. When calcination temperature reached 900 ºC, Only rutile phase was present. As seen in the figure, MB photocatalytic degradation increases from 12% to 19% with the calcination temperature. At this acid and water ratios, it seems that the degradation activity increases if there is only rutile phase present in TiO_2. Even though the crystallite size of

rutile for TiO_2 calcined at 700 and 900 ^oC is almost the same, 120 nm and 127 nm, the degradation acitivty is ~58% higher for the sample calcined at 900 ^oC (having 127 nm crystallite size). This seems to indicate that the presence of anatase phase in TiO_2 lowers the activity for the same crystallite size of rutile.

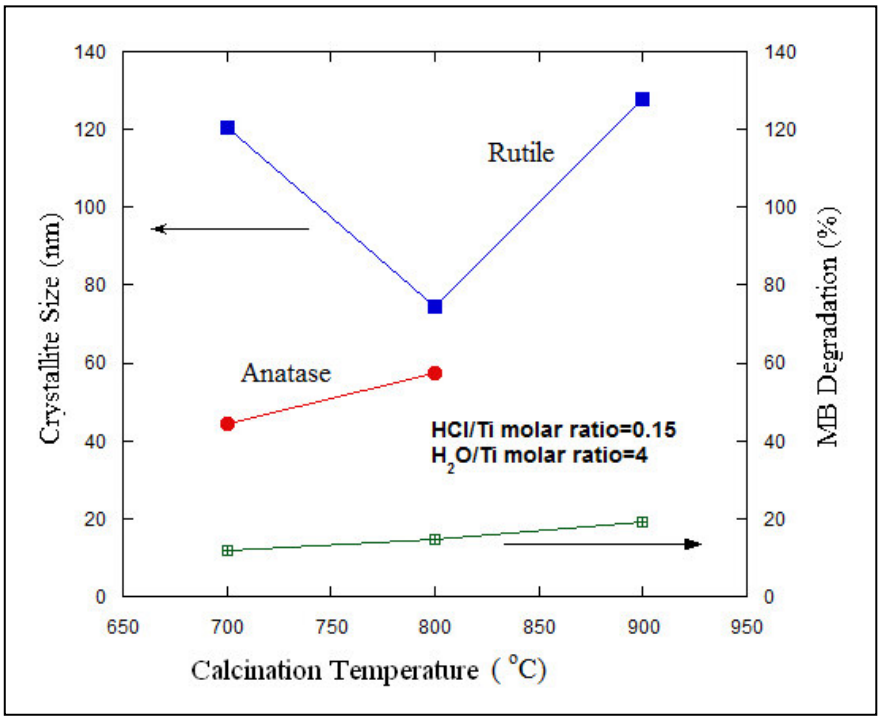

Figure 4.21. Relation between the crystallite size, H_2O/Ti molar ratio and MB % degradation for the sample of TiO_2-w:4-a:0.15-T:600, TiO_2-w:5-a: 0.15-T:600 and TiO_2-w:5.6-a:0.15-T:600

TiO_2 photocatalysts having only rutile phase showed high degradation activity at the same acid ratio of 0.15 and 900 ^oC calcination temperature. When 0.45 of HCl/Ti ratio instead of 0.15 acid ratio and 900 ^oC of the calcination temperature was used in the preparation of TiO_2, 25% MB degradation was obtained. It seems that this slight increase of degradation may be due to decrease of rutile crystallite size as seen in Table 4.6. Since two TiO_2 photocatalysts; TiO_2-w:4-a:0.45-T:900 and TiO_2-w:4-a:0.15-T:900, have almost the same direct band gap energies, 3.09 and 3.04, respectively, the slight increase of degradation activity seems to be dependent on the rutile crystallite size. In fact, smaller the rutile crystallite size, higher the degradation activity. High acid ratio used in the preparation resulted in decrease of rutile crystallite size similar to anatase crystallite size change as a function of acid ratio as seen in Figure 4.19. Generally, anatase phase of TiO_2 have been found to be more active than rutile phase

(Sun et al. 2003). However, in this study, rutile phases of TiO_2 samples were found to be more active than anatase phase. This results could be explained by the dominant photocatalytic path occurred through indirect band gap rather than direct band gap but this needs to be studied in details.

Table 4.6. Photocatalytic efficiencies and crystallite sizes of TiO_2 samples

Pure TiO_2 Catalysts	**% Degradation of MB**	**Crystallite size (nm)**
TiO2-w:4-a:0.45-T:900	25	87
TiO2-w:4-a:0.15-T:900	19.03	127

Additionally, in this thesis, photocatalytic degradation of commercial TiO_2 (from Degussa Inc.) was studied at the same reaction conditions. Photocatalytic degradation obtained using Degussa was 30%. Since Degussa TiO_2 is very fine powder and dispersed very well in the methylene blue, the higher degradation activity was obtained. In fact, the reaction medium was not stirred; thus, leading to mass transfer limitations and lower activities. This is also clearly seen in Figure 4.22 when photocatalytic degradation of TiO_2-w:4-a:0.45-T:900 sample which showed 25% degradation were studied as a function of the reaction time.

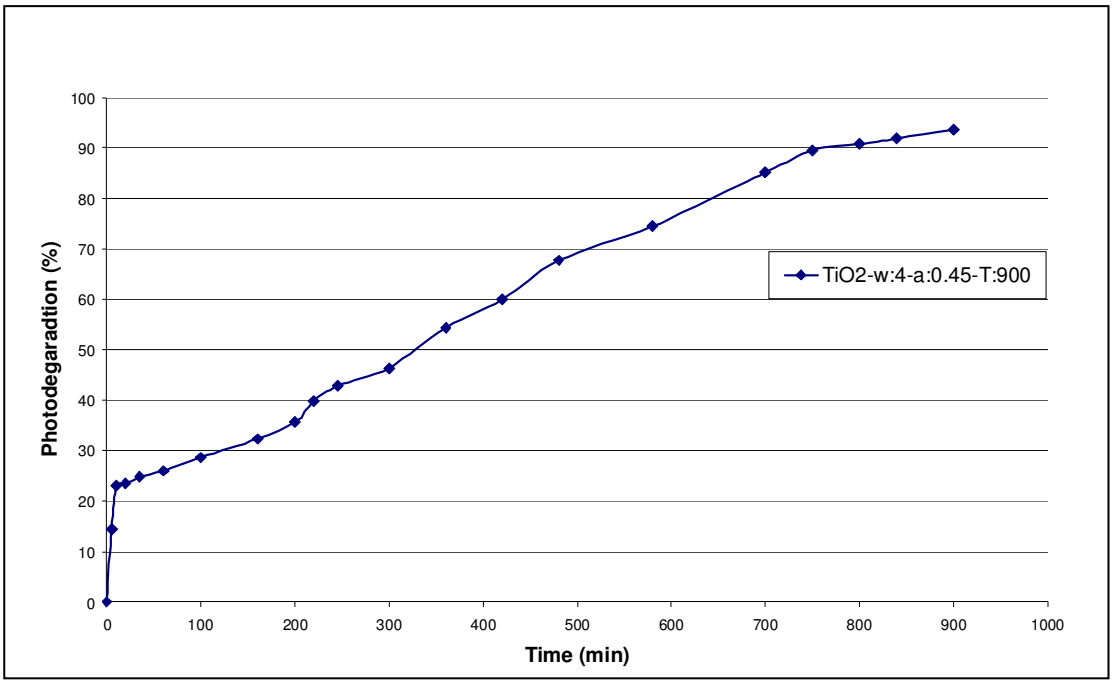

Figure 4.22. Photocatalytic degradation versus time graph for TiO_2-w:4-a:0.45-T:900

The degradation showed a sharp increase as the reaction time increased to 35 min and after that, the degradation almost linearly increased with the reaction time. This behavior seems to indicate the effect of mass transfer limitations. In fact, this is plausible since the content of the system was not stirred.

Photocatalytic activity of Fe^{3+} doped TiO_2 were found to be much lower than pure TiO_2 and also, there was significant leaching of iron ions during the photocatalytic degradation activity tests. Therefore, the sound comparison between doped TiO_2 samples and also between undoped and doped TiO_2 was not possible.

CHAPTER 5

CONCLUSIONS

In this thesis, pure TiO_2 and Fe^{3+} doped TiO_2 photocatalysts were synthesized. Then, the synthesized TiO_2 samples were characterized using XRD and DR spectroscopy techniques. It was found that the anatase-to-rutile phase transformation occurred between 700-800 ºC in this study. TiO_2 samples prepared with H_2O/Ti ratio of 4 and HCl/Ti ratio of 0.15 at 900 ^oC and TiO_2 samples prepared with H_2O/Ti ratio of 4 and HCl/Ti ratio of 0.45, at 900 ^oC had only rutile phase. Fe^{3+} doping did not affect the type of crystalline phase formation but affected on the crystallite size of TiO_2. A small amount of Fe^{3+} doping caused smaller TiO_2 crystallite size than pure TiO_2. When doping was increased, the TiO_2 crystallite size also increased. Moreover, TiO_2 crystallite sizes increased with increasing of calcination temperature, due to sintering of TiO_2 particles. Also, increasing amount of water in TiO_2 sol-gel preparation resulted in smaller crystallite sizes.

Band gap energies of the TiO_2 samples were calculated using Kubelka-Munk function and Polymath software. The results showed that the samples with rutile phase had small band gap energies. The smallest band gap energy, 3.02 eV, was obtained for TiO_2-w:4-a:0.45-T:900 sample. Photocatalytic activity measurement on this sample showed the maximum photocatalytic degradation of 25% in 10 min. However, doping TiO_2 with Fe did not result in higher photocatalytic activity and also the significant leaching of iron ion was observed. High degradation activity is obtained when the crystalline phase is rutile and the rutile crystallite size is 86 nm. Also, pure anatase phase was found to be not as active as the rutile phase. These may be explained with the oxygen defect sites created on the TiO_2 surface during the preparation, which may lead to very active TiO_2 with smaller indirect band gap energy. This needs to be further studied in details. Besides, time on stream analysis of TiO_2-w:4-a:0.45-T:900 revealed the presence of mass transfer limitations and hence, it took 15 h to reach 93% degradation.

REFERENCES

Al-Salim, N. I., Bagshaw, S. A., Bittar, A., Kemmitt, T., McQuillan, A. J., Millsa, A. M., and Ryan, M. J., 2000 ‘‘Characterisation and activity of sol-gel-prepared TiO_2 photocatalysts modified with Ca, Sr or Ba ion additives’’ *Journal of Materials Chemistry*, 2000, 2358-2363

Banerjee, A. N., 2011 ‘‘The design, fabrication, and photocatalytic utility of nanostructured semiconductors: focus on TiO2-based nanostructures’’ *Nanotechnology, Science and Applications* 2011:4 35–65

Brinker, G. J., Scherer, G. W., 1990 ‘‘Sol-Gel Science: The Physics and Chemistry of Sol-Gel Processing’’ *Academic Press Inc.*, pp. 11-20

Chan, C. K., Porter, J. F., Li, Y. G., Guo, W. and Chan, C. M., 1998 ‘‘Effects of Calcination on the Microstructures and Photocatalytic Properties of Nanosized Titanium Dioxide Powders Prepared by Vapor Hydrolysis’’ *Journal of the American Ceramic Society* Vol. 82 No. 3 (1999) 566–72

Colmenares, J. C., Luque, R., Campelo, J. M., Colmenares, F., Karpiński, Z., and Romero, A. A., 2009 ‘‘Nanostructured Photocatalysts and Their Applications in the Photocatalytic Transformation of Lignocellulosic Biomass: An Overview’’ *Materials* 2009, *2*, 2228-2258

El-Bahy, Z. M., Ismail, A. A., Mohamed, R. M., 2008 ‘‘Enhancement of titania by doping rare earth for photodegradation of organic dye (Direct Blue)’’ *Journal of Hazardous Materials* 166 (2009) 138–143

Ertl, G., Knözinger, H., Schüth, F., Weitkamp, J., 2008. ‘‘Handbook of Heterogeneous Catalysis’’ 2nd Edition, Wiley-VCH Verlag GmbH & Co. KGaA, pp. 119-122

Hasan, M. M., Haseeb, A. S. M. A., Saidur, R., and Masjuki, H. H., 2008 *''Effects of Annealing Treatment on Optical Properties of Anatase TiO_2 Thin Films'' International Journal of Chemical and Biological Engineering* 1:2 2008

Hsiung, T. L., Wanga, H. P., Linc, H. P., 2007 ''Chemical structure of photocatalytic active sites in nanosize TiO_2'' *Journal of Physics and Chemistry of Solids* 69 (2008) 383–385

Jian-xiao, L. V., Ying, C., Guo-hong, X., Ling-yun, Z., and Su-fen, W., 2011, ''Decoloration of methylene blue simulated wastewater using a UV-H_2O_2 combined system'' *Journal of Water Reuse and Desalination* 2011

Leary, R., Westwood, A., 2010 ''Carbonaceous nanomaterials for the enhancement of TiO_2 Photocatalysis'' *Carbon* 49 (2011) 741-772

Liqiang, J., Xiaojun, S., Weimin, C., Zili, X., Yaoguo, D., Honggang, F., 2002 ''The preparation and characterization of nanoparticle TiO_2/Ti films and their photocatalytic activity'' *Journal of Physics and Chemistry of Solids* 64 (2003) 615–623

Park, J. Y., Lee, C., Jung, K. W., and Jung, D., 2008 ''Structure Related Photocatalytic Properties of TiO_2'' *Bull. Korean Chem. Soc.* 2009 Vol. 30 No. 2

Paola, A., Garcìa-López, E., Marcì, G., Martìn, Palmisano, C. L., Rives, V., Venezia, A. M., 2003 ''Surface characterisation of metal ions loaded TiO_2 photocatalysts: structure–activity relationship'' *Applied Catalysis B: Environmental* 48 (2004) 223–233

Qiu, K., Zhang, C., Li, J., Li, Q., Zhao, J., 2007 ''Photocatalytic Degradation of NO_2^- by Fe^{3+}-Doped TiO_2 Nano Particles Prepared by Sol-Gel Method'' *Materials Science Forum* Vols. 544-545 (2007) pp 111-114

Salem , I. A., El-Maazawi, M. S., ‘‘Kinetics and Mechanism of Color Removal of Methylene Blue with Hydrogen Peroxide Catalyzed by Some Supported Alumina Surfaces’’ *Chemosphere* 41 (2000), 1173-1180

Sayılkan, F., Asiltürk, M., Sener, S., Erdemoğlu, S., Erdemoğlu M., and Sayılkan, H., 2006 ‘‘Hydrothermal Synthesis, Characterization and Photocatalytic Activity of Nanosized TiO_2 Based Catalysts for Rhodamine B Degradation’’ *Turk J Chem* 31 (2007), 211 – 221

Sobczyński, A., Dobosz, A., 2001 ‘‘Water Purification by Photocatalysis on Semiconductors’’ *Polish Journal of Environmental Studies* Vol. 10, No. 4 (2001), 195-205

Su, C., Hong, B.-Y., Tseng, C.-M., 2004 ‘‘Sol–gel preparation and photocatalysis of titanium dioxide’’ *Catalysis Today* 96 (2004) 119–126

Sun, B., Smirniotis, P. G., 2003 ‘‘Interaction of anatase and rutile TiO_2 particles in aqueous photooxidation’’ *Catalysis Today* 88 (2003) 49–59

Sonawane, R. S., Kale, B. B., Dongare, M. K., 2003 ‘‘Preparation and photo-catalytic activity of Fe–TiO_2 thin films prepared by sol–gel dip coating’’ *Materials Chemistry and Physics* 85 (2004) 52–57

Song, L., Wu, Y., Lu, X., 2007 ‘‘Preparation and Characterization of Doped Nanometer TiO_2’’ *Advanced Materials Research* Vols. 26-28 (2007) pp. 649-652

Thiruvenkatachari, R., Vigneswaran S., and Moon, I. S., 2007 ‘‘A review on UV/TiO_2 photocatalytic oxidation process’’ *Korean J. Chem. Eng.* 25(1) 64-72 (2008)

Tseng, T. K., Lin,. S., Chen Y. J., and Chu, H., 2010 ‘‘A Review of Photocatalysts Prepared by Sol-Gel Method for VOCs Removal’’ *International Journal of Molecular Sciences* 2010, 11, 2336-2361

Torrent, J., Barrón, V., 2002 ‘‘Diffuse Reflectance Spectroscopy of Iron Oxides’’ *Encyclopedia of Surface and Colloid Science*

Vijayan, P., Mahendiran, C., Suresh, C., Shanthi, K., 2008 ‘‘Photocatalytic activity of iron doped nanocrystalline titania for the oxidative degradation of 2,4,6-trichlorophenol’’ *Catalysis Today* 141 (2009) 220–224

Wang, B., Li, Q., Wang, W., Li, Y., Zhai, J., 2010 ‘‘Preparation and characterization of Fe^{3+}-doped TiO_2 on fly ash cenospheres for photocatalytic application’’ *Applied Surface Science* 257 (2011) 3473–3479

Yu, J., Zhao, X., Zhao, Q., 2000, ‘‘Effect of surface structure on photocatalytic activity of TiO_2 thin films prepared by sol-gel method’’ *Thin Solid Films* 379 (2000) 7-14

Zhang, X., Zhou, G., Zhang, H., Wu, C., Song, H., 2011 ‘‘Characterization and activity of visible light–driven TiO_2 photocatalysts co-doped with nitrogen and lanthanum’’ *Transition Met Chem* (2011) 36:217–222

APPENDIX A

XRD SPECTRUMS AND CRYSTALLITE SIZES

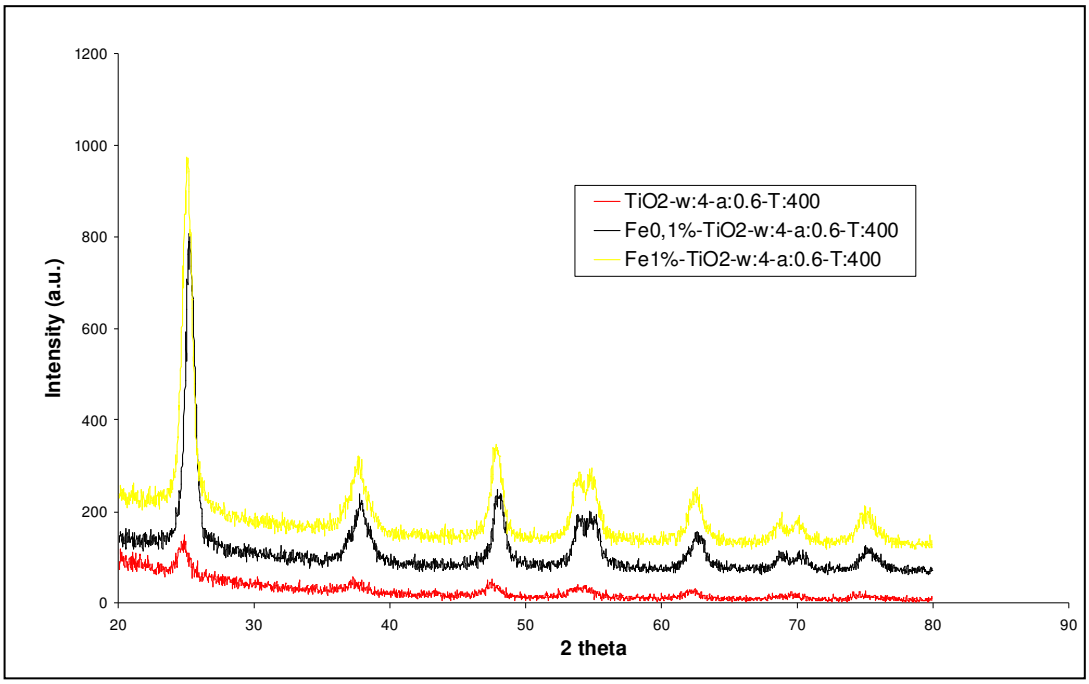

Figure A.1. XRD patterns of pure and 0.1 w.% and 1 w.% Fe^{3+} doped TiO_2-w:4-a:0.6-T:400 photocatalysts

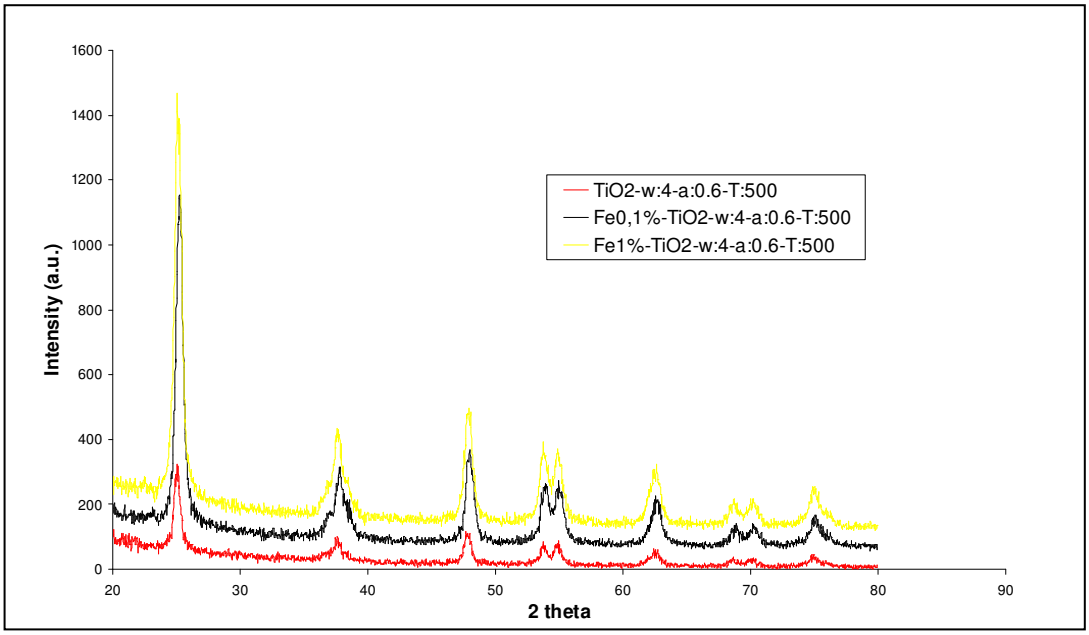

Figure A.2. XRD patterns of pure and 0.1 w.% and 1 w.% Fe^{3+} doped TiO_2-w:4-a:0.6-T:500 photocatalysts

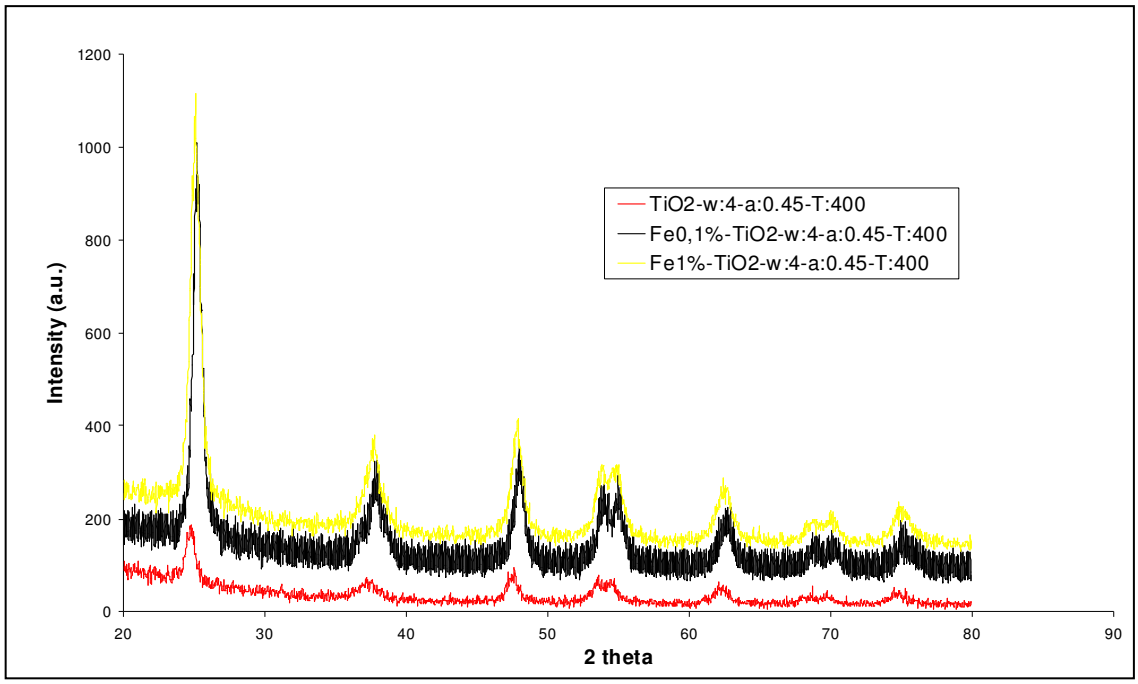

Figure A.3. XRD patterns of pure and 0.1 w.% and 1 w.% Fe^{3+} doped TiO_2-w:4-a:0.45 T:400 photocatalysts

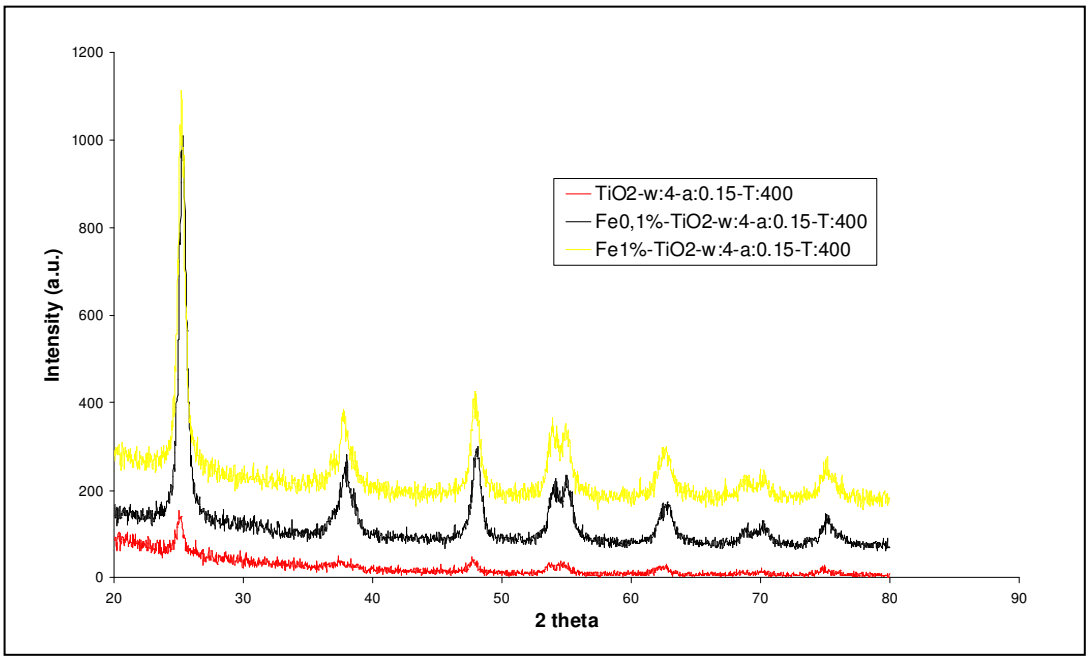

Figure A.4. XRD patterns of pure and 0.1 w.% and 1 w.% Fe^{3+} doped TiO_2-w:4-a:0.15-T:400 photocatalysts

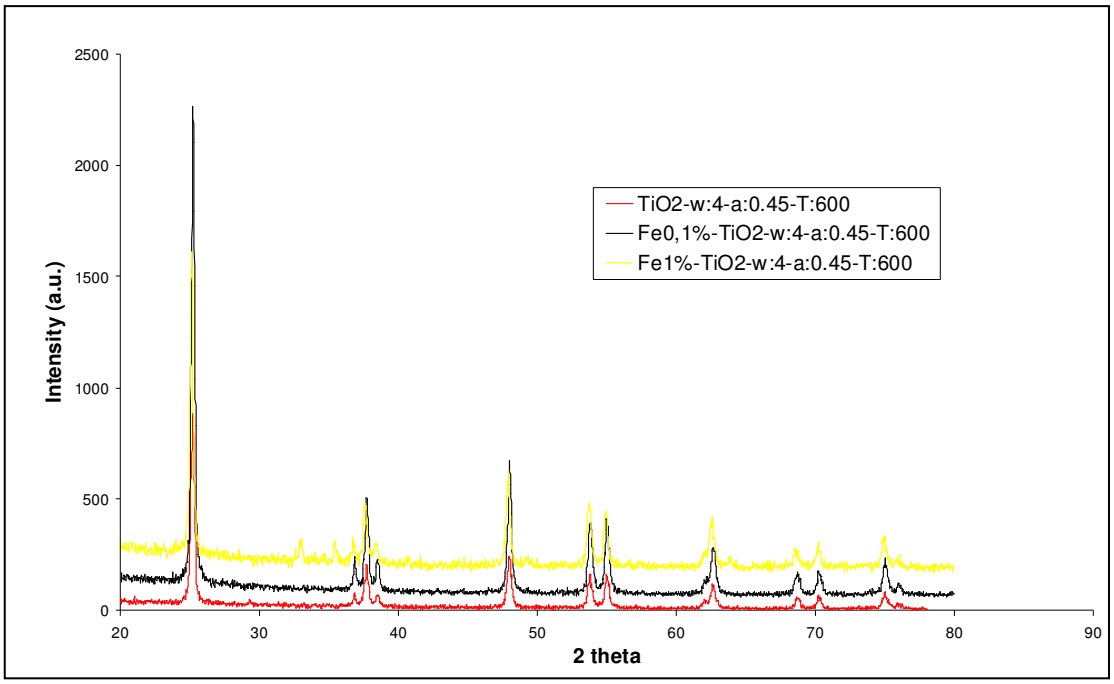

Figure A.5. XRD patterns of pure and 0.1 w.% and 1 w.% Fe^{3+} doped TiO_2-w:4-a:0.45-T:600 photocatalysts

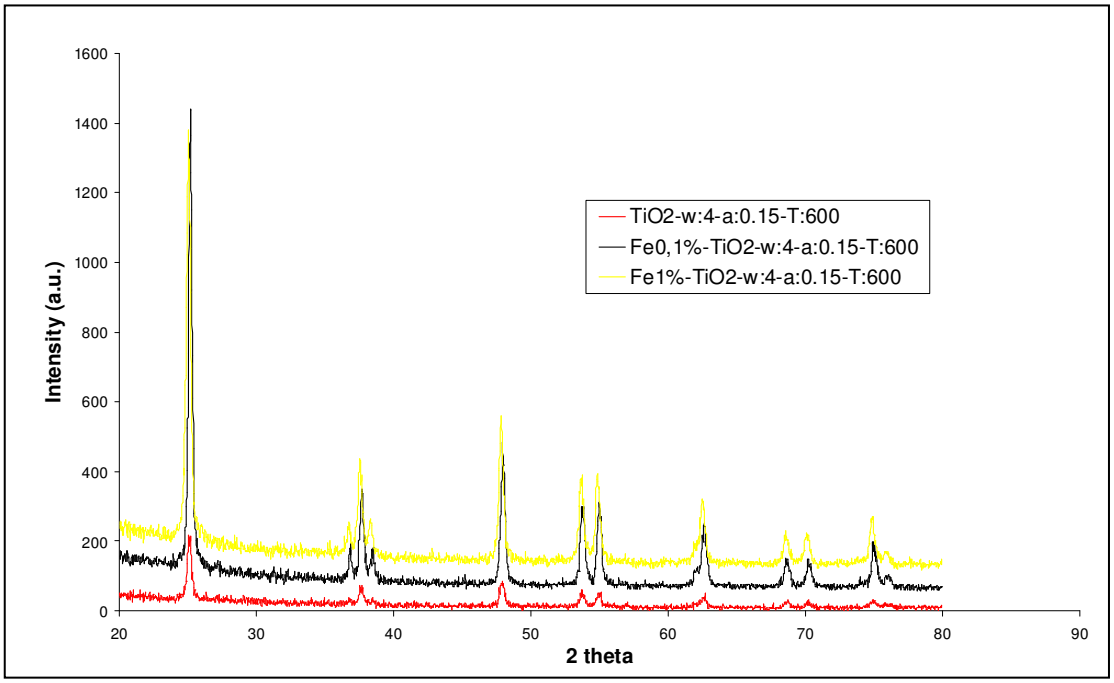

Figure A.6. XRD patterns of pure and 0.1 w.% and 1 w.% Fe^{3+} doped TiO_2-w:4-a:0.15 T:600 Photocatalysts

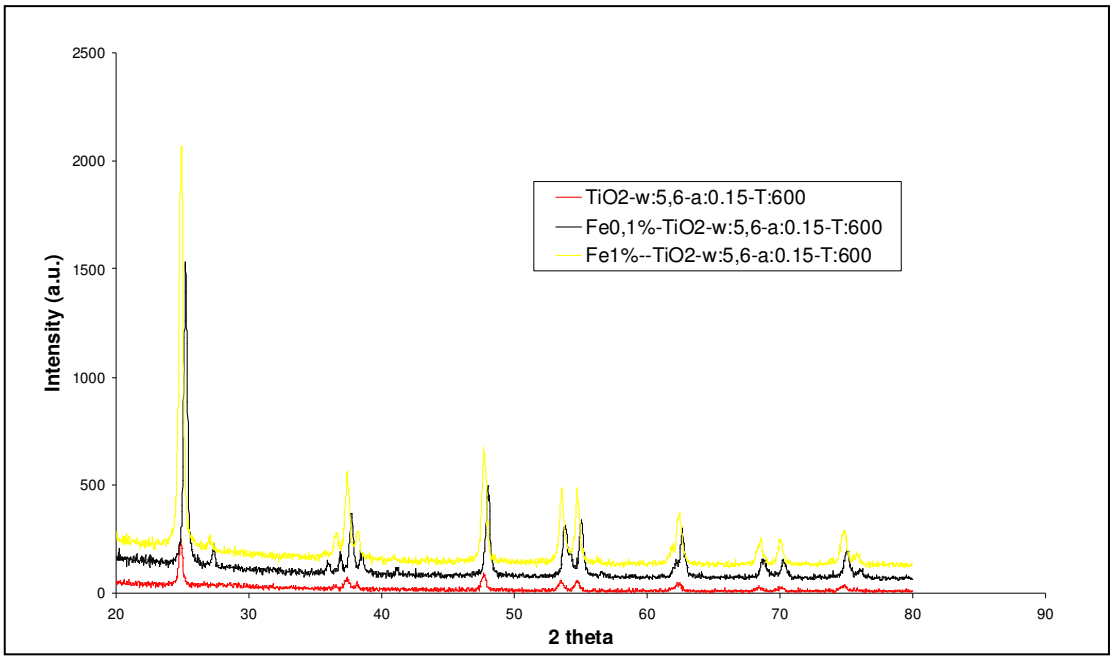

Figure A.7. XRD patterns of pure and 0.1 w.% and 1 w.% Fe^{3+} doped TiO_2-w:5,6-a:0.15 T:600 photocatalysts

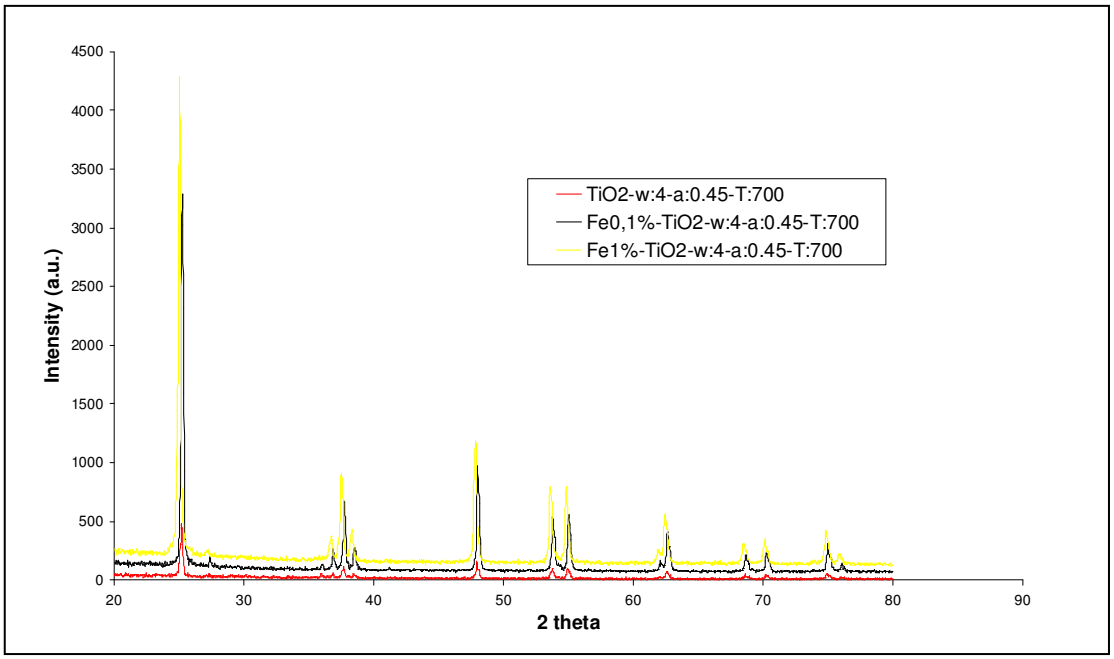

Figure A.8. XRD patterns of pure and 0.1 w.% and 1 w.% Fe^{3+} doped TiO_2-w:4-a:0.45-T:700 photocatalysts

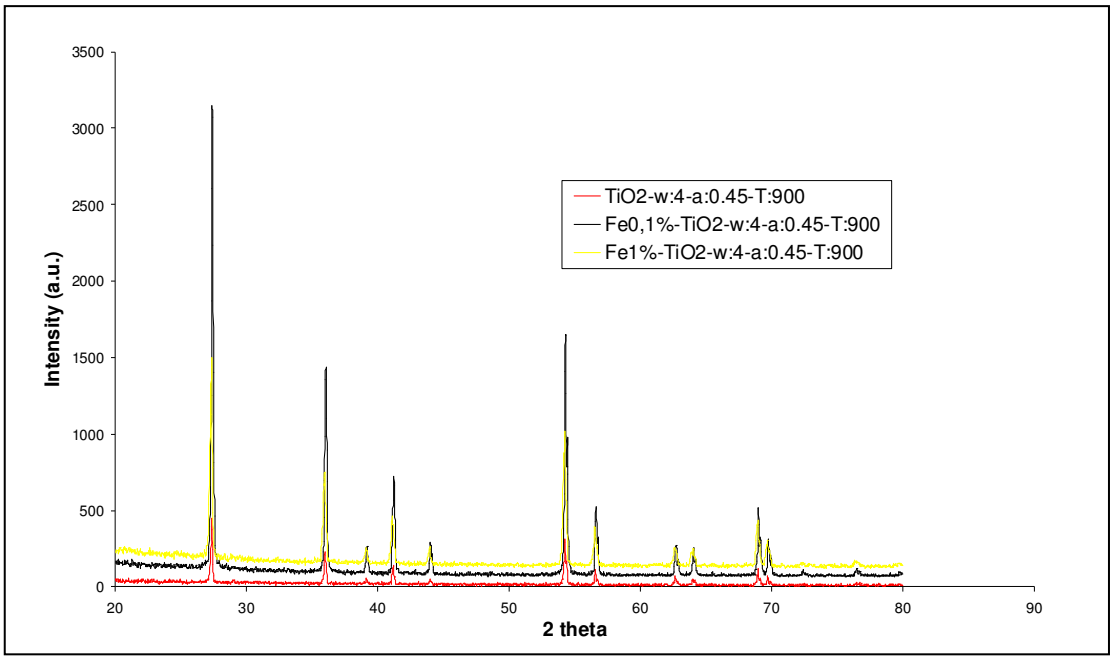

Figure A.9. XRD patterns of pure and 0.1 w.% and 1 w.% Fe^{3+} doped TiO_2-w:4-a:0.45 T:900 photocatalysts

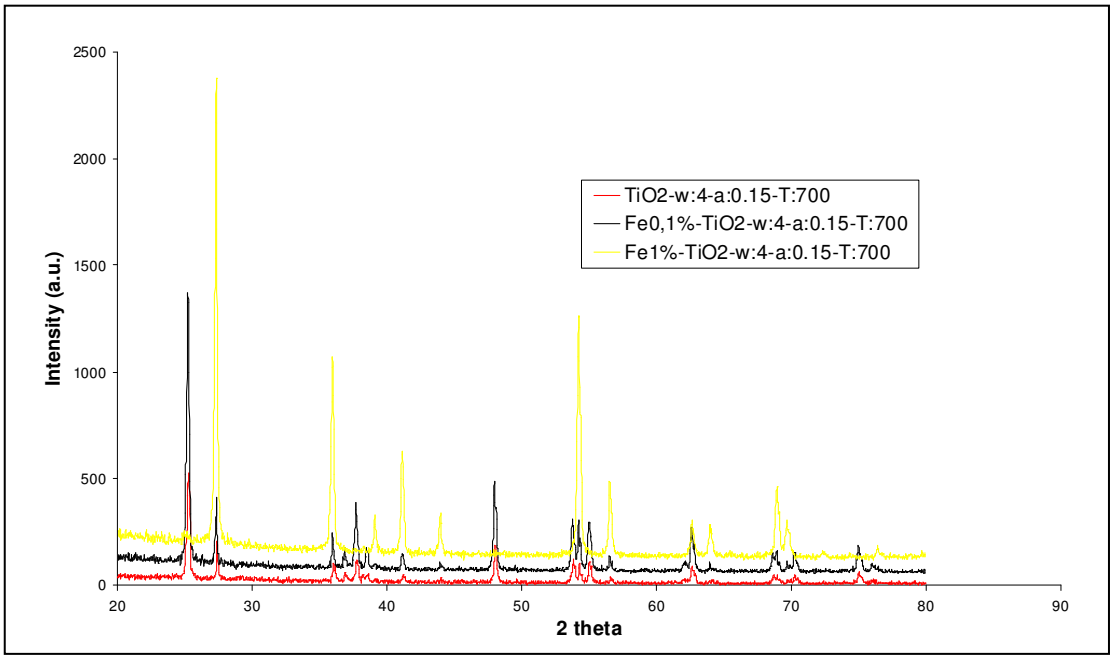

Figure A.10. XRD patterns of pure and 0.1 w.% and 1 w.% Fe^{3+} doped TiO_2-w:4-a:0.15-T:700 photocatalysts

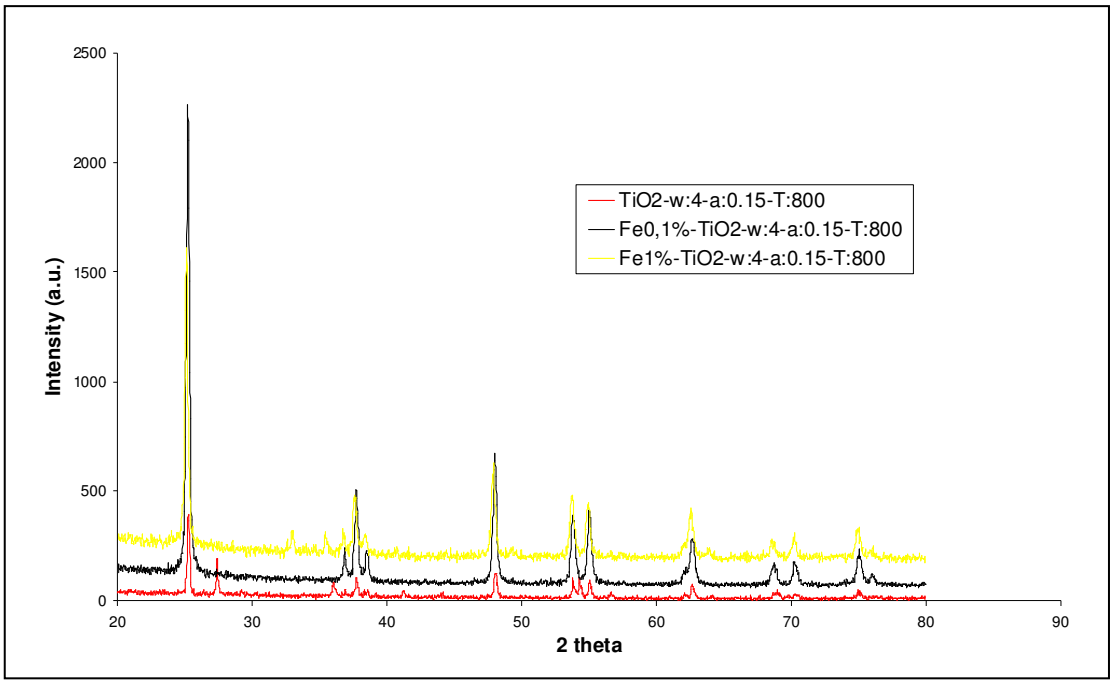

Figure A.11. XRD patterns of pure and 0.1 w.% and 1 w.% Fe^{3+} doped TiO_2-w:4-a:0.15- T:700 photocatalysts

Table A.1. Crystallite size of the TiO_2 and Fe^{3+} doped TiO_2 nanoparticles

Fe doped TiO_2 catalysts	Crystallite Size (nm)	Pure TiO_2 catalysts	Crystallite Size (nm)
Fe1%-TiO2-w:4-a:0.6-T:400	7.5	TiO2-w:4-a:0.6-T:400	13.2
Fe1%-TiO2-w:4-a:0.6-T:500	10.1	TiO2-w:4-a:0.6-T:400	12.5
Fe1%-TiO2-w:4-a:0.6-T:600	28.9	TiO2-w:4-a:0.6-T:500	21.5
Fe1%-TiO2-w:4-a:0.45-T:400	8.0	TiO2-w:4-a:0.6-T:600	38.6
Fe1%-TiO2-w:8-a:0.6-T:500	9.0	TiO2-w:4-a:0.45-T:400	15.9
Fe1%-TiO2-w:4-a:0.15-T:400	9.4	TiO2-w:4-a:0.6-T:500	15.7
Fe1%-TiO2-w:4-a:0.45-T:600	26.1	TiO2-w:5-a:0.6-T:500	13.7
Fe1%--TiO2-w:4-a:0.15-T:600	18.0	TiO2-w:8-a:0.6-T:500	11.7
Fe1%--TiO2-w:5.6-a:0.15-T:600	21.0	TiO2-w:4-a:0.3-T:400	12.9
Fe1%-TiO2-w:4-a:0.45-T:700	35.4	TiO2-w:4-a:0.2-T:400	16.2
Fe1%-TiO2-w:4-a:0.45-T:800	41.4	TiO2-w:4-a:0.15-T:400	21.3
Fe1%-TiO2-w:4-a:0.45-T:900	38.4	TiO2-w:4-a:0.45-T:600	26.7
Fe1%-TiO2-w:4-a:0.15-T:700	40.7	TiO2-w:4-a:0.15-T:600	26.7
Fe1%-TiO2-w:4-a:0.15-T:800	43.7	TiO2-w:5.6-a:0.15-T:600	24.7
Fe1%-TiO2-w:4-a:0.15-T:900	58.1	TiO2-w:5-a:0.15-T:600	26.3
Fe0.1%-TiO2-w:4-a:0.6-T:400	8.4	TiO2-w:4-a:0.45-T:700	39.6
Fe0.1%-TiO2-w:4-a:0.6-T:500	11.2	TiO2-w:4-a:0.45-T:800	51.6
Fe0.1%-TiO2-w:4-a:0.6-T:600	28.8	TiO2-w:4-a:0.45-T:900	52.1
Fe0.1%-TiO2-w:4-a:0.45-T:400	30.1	TiO2-w:4-a:0.15-T:700	33.6
Fe0.1%-TiO2-w:8-a:0.6-T:500	12.4	TiO2-w:4-a:0.15-T:800	41.2
Fe0.1%-TiO2-w:4-a:0.15-T:400	10.2	TiO2-w:4-a:0.15-T:900	58.6
Fe0.1%-TiO2-w:4-a:0.45-T:600	32.1		
Fe0.1%-TiO2-w:4-a:0.15-T:600	25.9		
Fe0.1%-TiO2-w:5.6-a:0.15-T:600	24.5		
Fe0.1%-TiO2-w:4-a:0.45-T:700	52.7		
Fe0.1%-TiO2-w:4-a:0.45-T:800	90.4		
Fe0.1%-TiO2-w:4-a:0.45-T:900	60.9		
Fe0.1%-TiO2-w:4-a:0.15-T:700	41.3		
Fe0.1%-TiO2-w:4-a:0.15-T:800	66.8		
Fe0.1%-TiO2-w:4-a:0.15-T:900	82.0		

APPENDIX B

DIFFUSE REFLECTANCE SPECTRUMS

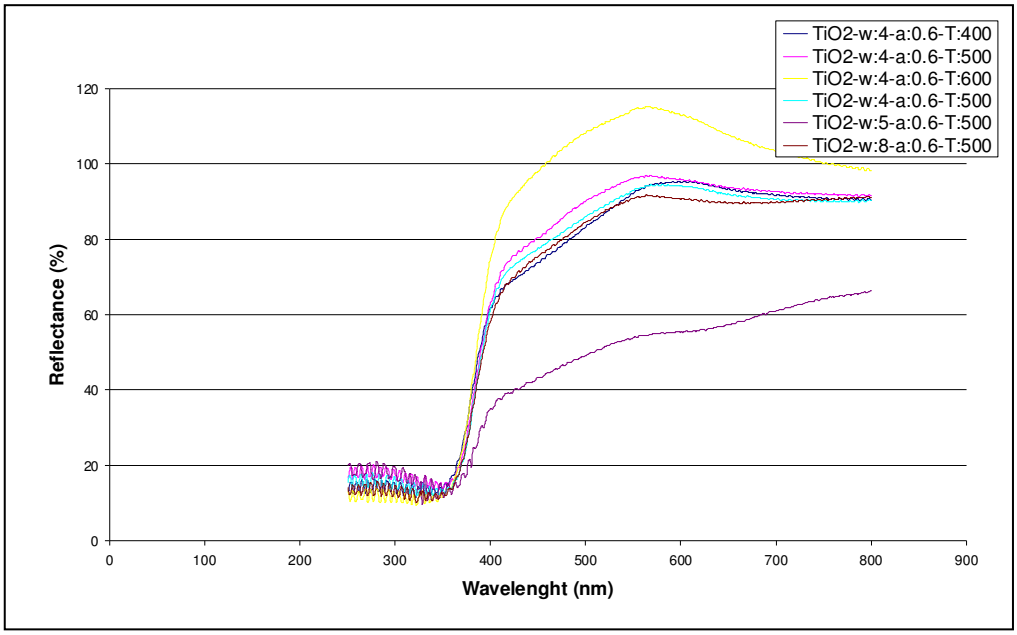

Figure B.1. DRS of TiO_2-w:4-a:0.6-T:400, TiO_2-w:4-a:0.6-T:500, TiO_2-w:4-a:0.6-T:600, TiO_2-w:4-a:0.6-T:500, TiO_2-w:5-a:0.6-T:500 and TiO_2-w:8-a:0.6 T:500

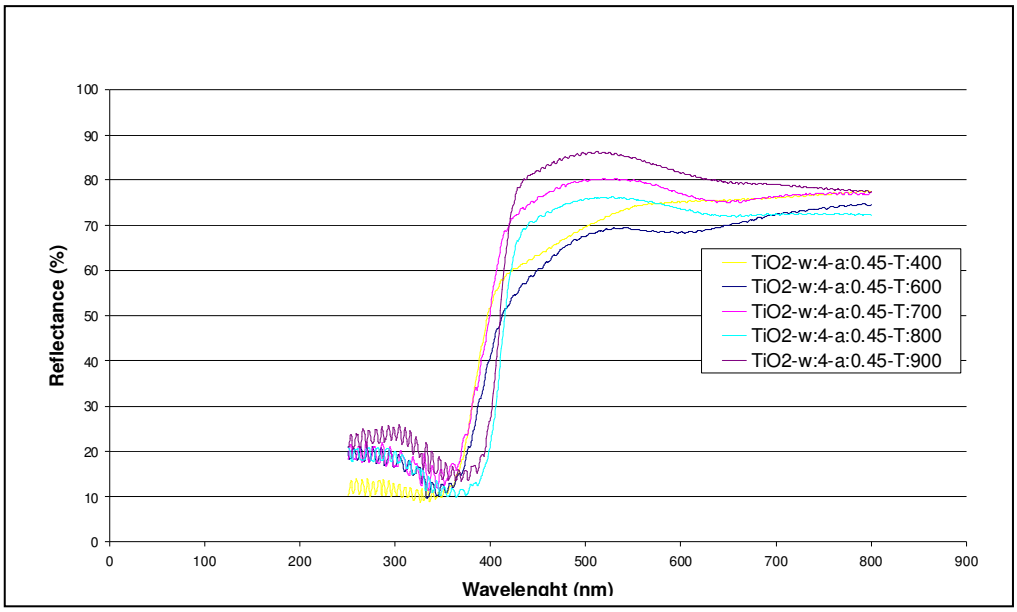

Figure B.2. DRS of TiO_2-w:4-a:0.45-T:400. TiO_2-w:4-a:0.45-T:400. TiO_2-w:4-a:0.45-T:600. TiO_2-w:4-a:0.45-T:700. TiO_2-w:4-a:0.4-T:800 and TiO_2-w:4-a:0.45-T:900

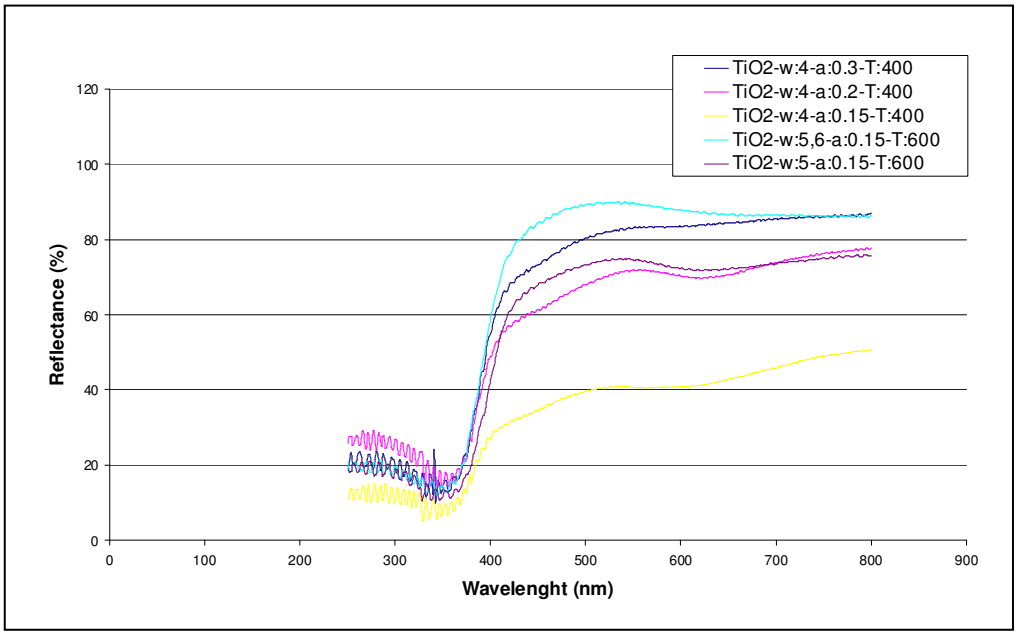

Figure B.3. Diffuse Reflectance Spectra of TiO_2-w:4-a:0.3-T:400, TiO_2-w:4-a:0.2-T:400, TiO_2-w:4-a:0.15-T:400, TiO_2-w:5.6-a:0.15-T:600 and TiO_2-w:5-a:0.15-T:600

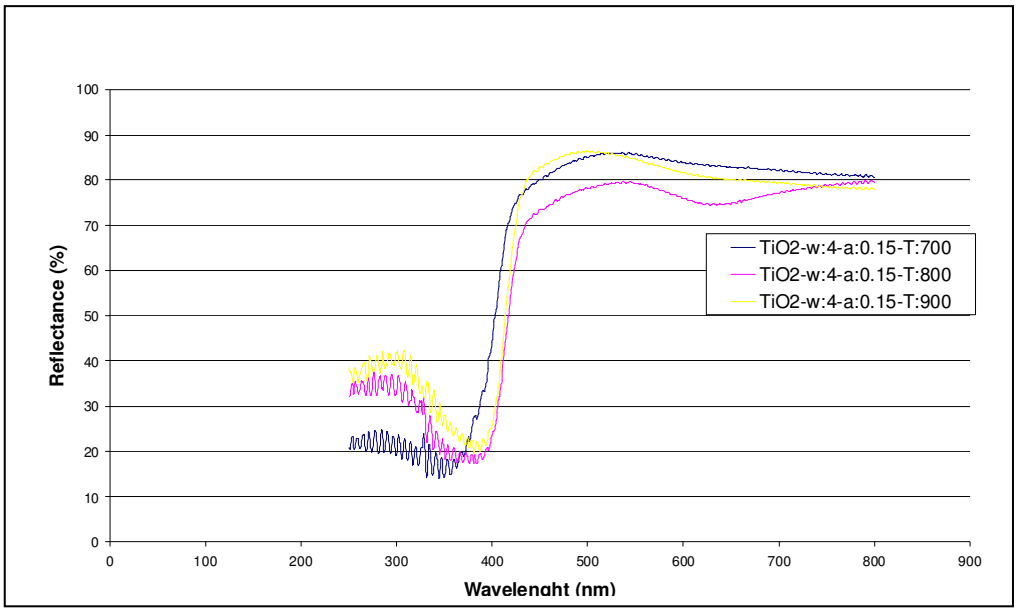

Figure B.4. Diffuse Reflectance Spectra of TiO_2-w:4-a:0.15-T:700, TiO_2-w:4-a:0.15-T:800 and TiO_2-w:4-a:0.15-T:900

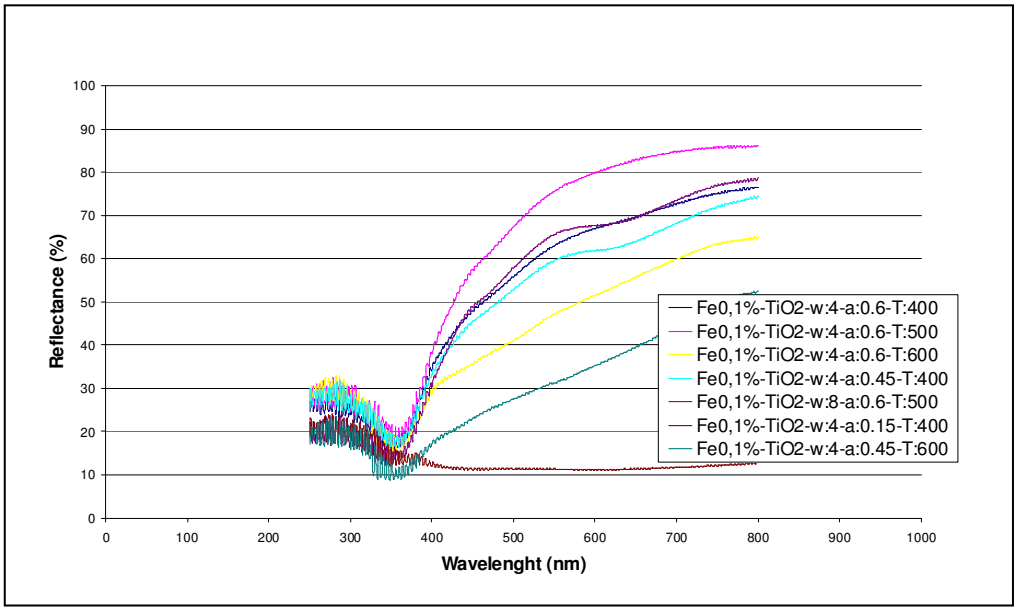

Figure B.5. Diffuse Reflectance Spectra of Fe0.1%-TiO_2-w:4-a:0.6-T:400, Fe0.1%-TiO_2-w:4-a:0.6-T:500, Fe0.1%-TiO_2-w:4-a:0.6-T:600, Fe0.1%-TiO_2-w:4-a:0.45-T:400, Fe0.1%-TiO_2-w:8-a:0.15-T:400 and Fe0.1%-TiO_2-w:4-a:0.45-T:600

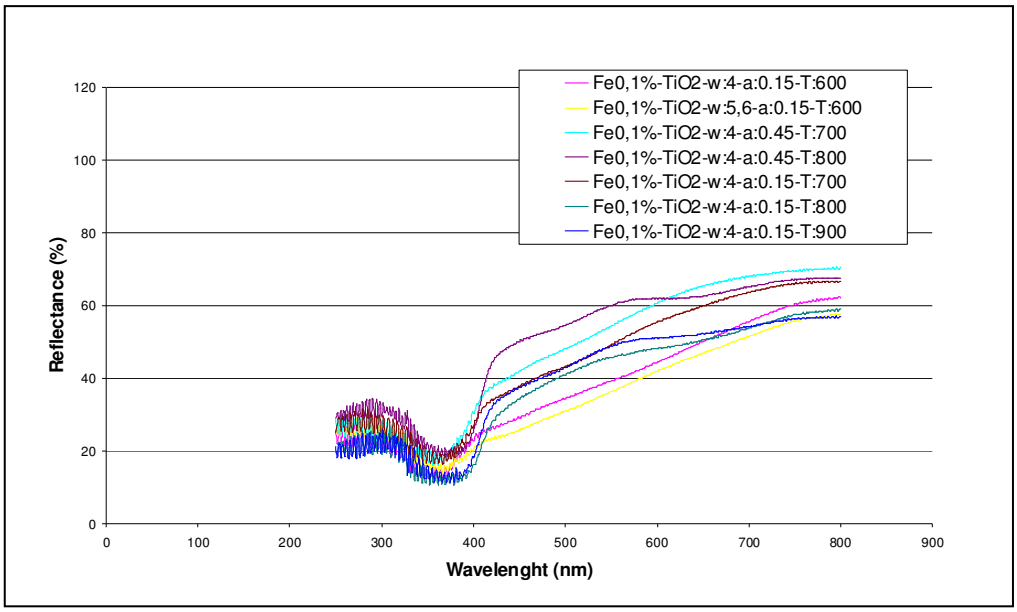

Figure B.6. Diffuse Reflectance Spectra of Fe0.1%-TiO_2-w:4-a:0.15-T:600, Fe0.1%-TiO_2-w:5.6-a:0.15-T:600, Fe0.1%-TiO_2-w:4-a:0.45-T:700, Fe0.1%-TiO_2-w:4-a:0.45-T:800, Fe0.1%-TiO_2-w:4-a:0.15-T:700, Fe0.1%-TiO_2-w:4-a:0.15-T:800 and Fe0.1%-TiO_2-w:4-a:0.15-T:900

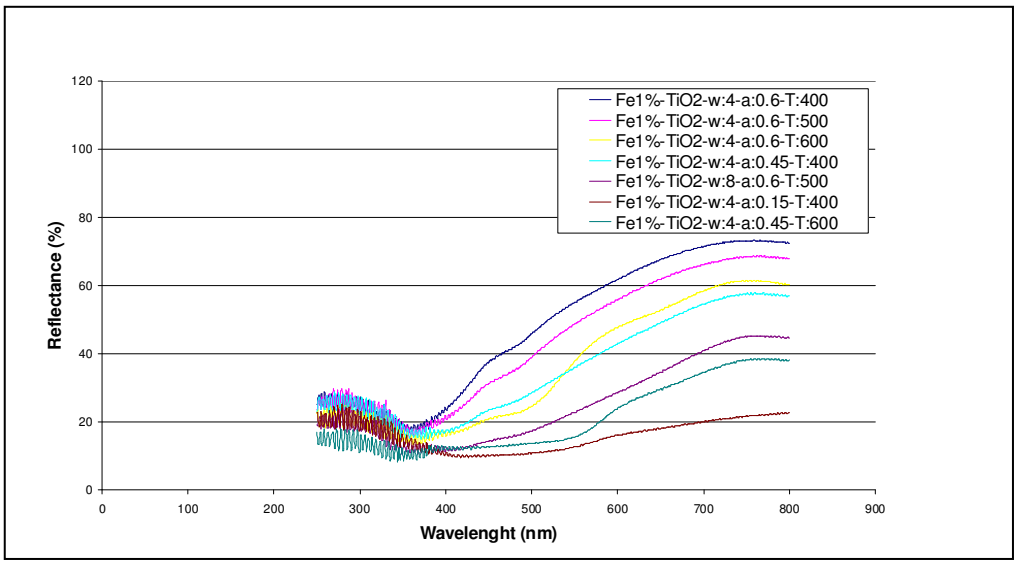

Figure B.7. Diffuse Reflectance Spectra of Fe1%-TiO_2-w:4-a:0.6-T:400, Fe1%-TiO_2-w:4-a:0.6-T:500, Fe1%-TiO_2-w:4-a:0.6-T:600, Fe1%-TiO_2-w:4-a:0.45-T:400, Fe1%-TiO_2-w:8-a:0.15-T:400 and Fe1%-TiO_2-w:4-a:0.45-T:600

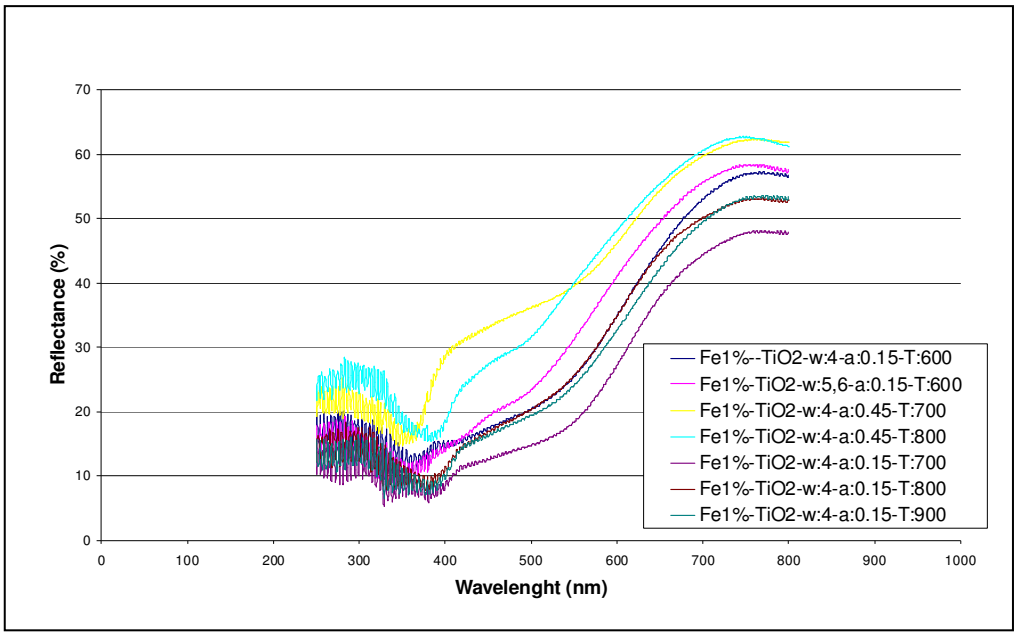

Figure B.8. Diffuse Reflectance Spectra of Fe1%-TiO_2-w:4-a:0.15-T:600,Fe1%-TiO_2-w:5.6-a:0.15-T:600, Fe1%-TiO_2-w:4-a:0.45-T:70, Fe1%-TiO_2-w:4-a:0.45-T:800, Fe1%-TiO_2-w:4-a:0.15-T:700, Fe1%-TiO_2-w:4-a:0.15-T:800 and Fe1%-TiO_2-w:4-a:0.15-T:900